

Hypertonic Stress Causes Cytoplasmic Translocation of Neuronal, but Not Astrocytic, FUS due to Impaired Transportin Function

Eva-Maria Hock, Zuzanna Maniecka, Marian Hruska-Plochan, Stefan Reber, Florent Laferrière, Sonu Sahadevan M K, Helena Ederle, Lauren Gittings, Lucas Pelkmans, Luc Dupuis, et al.

▶ **To cite this version:**

Eva-Maria Hock, Zuzanna Maniecka, Marian Hruska-Plochan, Stefan Reber, Florent Laferrière, et al.. Hypertonic Stress Causes Cytoplasmic Translocation of Neuronal, but Not Astrocytic, FUS due to Impaired Transportin Function. Cell Reports, 2018, 24 (4), pp.987-1000.e7. 10.1016/j.celrep.2018.06.094 . inserm-03376140

HAL Id: inserm-03376140

https://inserm.hal.science/inserm-03376140

Submitted on 13 Oct 2021

HAL is a multi-disciplinary open access archive for the deposit and dissemination of scientific research documents, whether they are published or not. The documents may come from teaching and research institutions in France or abroad, or from public or private research centers.

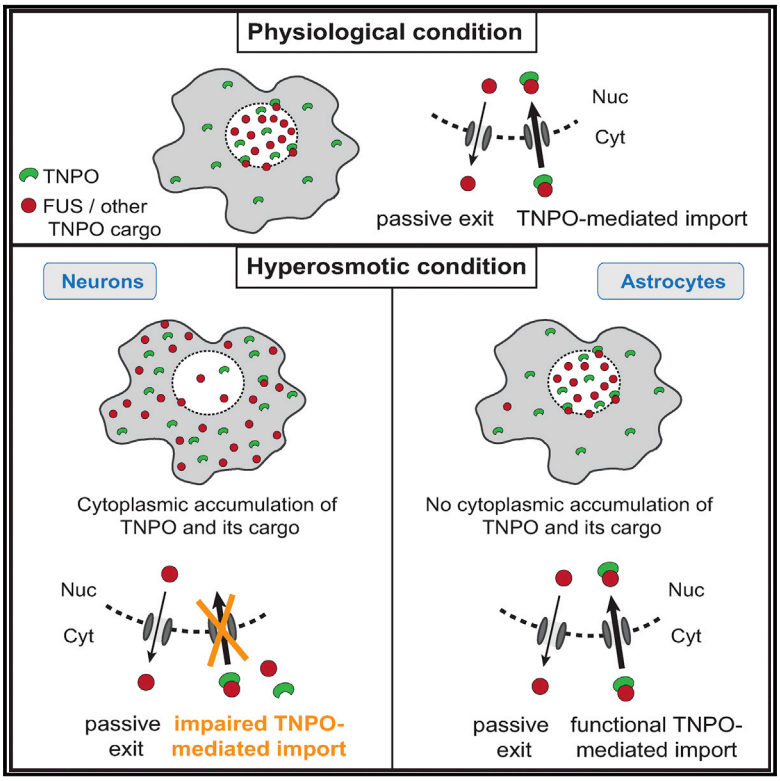
L'archive ouverte pluridisciplinaire **HAL**, est destinée au dépôt et à la diffusion de documents scientifiques de niveau recherche, publiés ou non, émanant des établissements d'enseignement et de recherche français ou étrangers, des laboratoires publics ou privés.

Article

Cell Reports

Hypertonic Stress Causes Cytoplasmic Translocation of Neuronal, but Not Astrocytic, FUS due to Impaired Transportin Function

Graphical Abstract



Highlights

- Hypertonic stress drives cytoplasmic relocation of endogenous FUS in neurons
- FUS shifts to the cytoplasm independently of stress granules or hyperosmolar pathways
- FUS translocation results from insufficient nuclear import by transportin
- Astrocytes are spared from stress-induced FUS translocation and pathology in FTD-FUS

Authors

Eva-Maria Hock, Zuzanna Maniecka, Marian Hruska-Plochan, ..., Marc-David Ruepp, Dorothee Dormann, Magdalini Polymenidou

Correspondence

magdalini.polymenidou@imls.uzh.ch

In Brief

Hock et al. show that hypertonic stress leads to cytoplasmic translocation and loss of function of neuronal FUS in a stress granule-independent manner. Stress-induced FUS translocation results from impaired Transportin-mediated nuclear import. Astrocytes are resistant to cytoplasmic FUS mislocalization upon hypertonic pressure and lack pathological protein accumulations in FTD-FUS brains.

Hock et al., 2018, Cell Reports *24*, 987–1000
July 24, 2018 © 2018 The Author(s).
https://doi.org/10.1016/j.celrep.2018.06.094

CellPress

Cell Reports
Article

OPEN ACCESS
CellPress

Hypertonic Stress Causes Cytoplasmic Translocation of Neuronal, but Not Astrocytic, FUS due to Impaired Transportin Function

Eva-Maria Hock,[1,2] Zuzanna Maniecka,[1,2] Marian Hruska-Plochan,[1] Stefan Reber,[3,4] Florent Laferrière,[1] Sonu Sahadevan M.K.,[1,2] Helena Ederle,[5,6,7] Lauren Gittings,[8] Lucas Pelkmans,[1] Luc Dupuis,[9] Tammaryn Lashley,[8] Marc-David Ruepp,[10] Dorothee Dormann,[5,6,7] and Magdalini Polymenidou[1,2,11,*]

[1]Institute of Molecular Life Sciences, University of Zurich, Winterthurerstrasse 190, 8057 Zurich, Switzerland
[2]Life Science Zurich Graduate School, University of Zurich and ETH Zurich, Zurich, Switzerland
[3]Department of Chemistry and Biochemistry, University of Bern, Bern, Switzerland
[4]Graduate School for Cellular and Biomedical Sciences, University of Bern, Bern, Switzerland
[5]BioMedical Center (BMC), Ludwig-Maximiians-University Munich, 82152 Planegg-Martinsried, Germany
[6]Graduate School of Systemic Neurosciences (GSN), 82152 Planegg-Martinsried, Germany
[7]Munich Cluster for Systems Neurology (SyNergy), 81377 Munich, Germany
[8]Queen Square Brain Bank for Neurological Diseases, Department of Molecular Neuroscience, UCL Institute of Neurology, London WC1N 1PJ, UK
[9]Faculty of Medicine, INSERM UMR-S1118 and Fédération de Médecine Translationnelle, Université de Strasbourg, Strasbourg, France
[10]UK Dementia Research Institute Centre at King's College London, Institute of Psychiatry, Psychology and Neuroscience, King's College London, Maurice Wohl Clinical Neuroscience Institute, 125 Coldharbour Lane, London SE5 9NU, UK
[11]Lead Contact
*Correspondence: magdalini.polymenidou@imls.uzh.ch
https://doi.org/10.1016/j.celrep.2018.06.094

SUMMARY

The primarily nuclear RNA-binding protein FUS (fused in sarcoma) forms pathological cytoplasmic inclusions in a subset of early-onset amyotrophic lateral sclerosis (ALS) and frontotemporal dementia (FTD) patients. In response to cellular stress, FUS is recruited to cytoplasmic stress granules, which are hypothesized to act as precursors of pathological inclusions. We monitored the stress-induced nucleocytoplasmic shuttling of endogenous FUS in an *ex vivo* mouse CNS model and human neural networks. We found that hyperosmolar, but not oxidative, stress induced robust cytoplasmic translocation of neuronal FUS, with transient nuclear clearance and loss of function. Surprisingly, this reaction is independent of stress granule formation and the molecular pathways activated by hyperosmolarity. Instead, it represents a mechanism mediated by cytoplasmic redistribution of Transportin 1/2 and is potentiated by transcriptional inhibition. Importantly, astrocytes, which remain unaffected in ALS/FTD-FUS, are spared from this stress reaction that may signify the initial event in the development of FUS pathology.

INTRODUCTION

The RNA/DNA-binding protein FUS (fused in sarcoma) has been implicated in the pathogenesis of two devastating neurodegenerative diseases, amyotrophic lateral sclerosis (ALS) (Kwiatkowski et al., 2009; Vance et al., 2009) and frontotemporal dementia (FTD) (Neumann et al., 2009). ALS is characterized by progressive paralysis due to motor neuron degeneration, whereas FTD patients suffer from cognitive impairment, caused by atrophy of the frontal and temporal brain lobes. Despite distinct symptoms, both diseases are clinically, pathologically, and genetically linked, and have possible common underlying causes, involving aberrant localization and aggregation of RNA-binding proteins (Ling et al., 2013).

FUS is a ubiquitously expressed ribonucleoprotein (RNP) with several RNA-binding domains that allow its involvement in various steps of RNA metabolism (Lagier-Tourenne et al., 2010). FUS regulates splicing events important for neuronal maintenance (Lagier-Tourenne et al., 2012), by associating with multiple spliceosomal complexes (Rappsilber et al., 2002; Zhou et al., 2002), such as the minor spliceosome (Reber et al., 2016) and nuclear splicing speckles (Meissner et al., 2003).

An atypical nuclear localization signal (PY-NLS) retains FUS predominantly in the nucleus via its interaction with the nuclear import receptors Transportin 1 and 2 (collectively called TNPO) (Dormann et al., 2010; Zhang and Chook, 2012). However, FUS is a shuttling protein that performs additional cytoplasmic functions, including regulation of axonal mRNA transport and local translation (Ederle and Dormann, 2017). The N-terminal region of FUS comprises a low complexity region (LCR) involved in protein-protein interactions, which renders the protein highly aggregation prone (Sun et al., 2011) and is predicted to attain prion-like properties (Cushman et al., 2010). In disease, FUS forms cytoplasmic inclusions in neurons and some types of glial cells, leading to reduction of available functional protein. Apart from loss of essential RNA processing functions, pathological mislocalization and aggregation may be toxic because of distorted RNA and protein interactions and mRNP (messenger RNP) dynamics (Bowden and Dormann, 2016).

This is an open access article under the CC BY license (http://creativecommons.org/licenses/by/4.0/).

Under stress conditions, cells form cytoplasmic stress granules (SGs), dynamic membrane-less organelles, which contain diverse tightly associated RNA-binding proteins (RBPs) with LCRs, including FUS (Anderson and Kedersha, 2009; Bentmann et al., 2012; Bosco et al., 2010; Dormann et al., 2010). SGs were hypothesized to act as precursors of aggregates, an idea strongly corroborated by the presence of other SG proteins in pathological FUS inclusions (Dormann et al., 2010) and by *in vitro* data showing that liquid-like FUS droplets mature over time from a dynamic to an aggregated state (Burke et al., 2015; Murakami et al., 2015; Patel et al., 2015). Nevertheless, no experimental demonstration of such a physiopathological transition within cells exists to date. Moreover, in the cellular context, nuclear compartmentalization of FUS would have to be overcome before conversion into cytoplasmic deposits occurs. In fact, SG recruitment was mostly demonstrated for FUS variants rendered artificially cytoplasmic, mimicking FUS-ALS cases. In these cases, mutations in the C-terminal PY-NLS disrupt binding to the nuclear import receptor TNPO1 (Dormann et al., 2010; Kwiatkowski et al., 2009; Vance et al., 2009), causing the initial cytoplasmic shift. In FTD-FUS cases, however, no *FUS* mutations have been found. Nonetheless, abnormal loss of arginine methylation of FUS, as well as coaggregation of FET proteins (EWS, TAF15) (Neumann et al., 2011) and their common import factor TNPO1 (Brelstaff et al., 2011), indicate a potential defect in nuclear shuttling.

Hyperosmolarity causes cell shrinkage due to osmosis-driven water efflux, and thus has many direct effects, such as elevated intracellular ionic strength and macromolecular crowding (Burg et al., 2007). SG formation due to hyperosmolar stress has been described to recruit exceptionally high levels of nuclear wild-type FUS in cell lines (Sama et al., 2013). However, it is unknown whether this response is recapitulated in the CNS and could thus provide a mechanism for FUS mislocalization to the cytoplasm independently of NLS mutations.

In this study, we sought to decipher the response of endogenous wild-type FUS to hyperosmotic stress in two systems mimicking the mouse and human brain environment. We found robust mislocalization of endogenous neuronal FUS with partial nuclear clearance due to hyperosmotic pressure, but not oxidative or other types of cellular stress. Surprisingly, FUS reactivity was independent of SG formation and occurred in a cell-type-specific manner, because astrocytic FUS was unaffected in these conditions. Furthermore, FUS exited the nucleus via passive diffusion rather than active export, and its redistribution was not driven by activation of the typical cellular osmotic stress-response pathways. Transcriptional inhibition potentiated the observed response, which involved cytoplasmic redistribution and reduced shuttling of TNPO during hyperosmotic stress. Other TNPO cargo proteins showed a similar response to FUS, whereas proteins shuttling independently of TNPO and other import receptors were unaffected. We propose that this phenomenon denotes a cellular mechanism for reducing nuclear activity of RBPs, through their rapid redistribution to the cytoplasm. Our findings have important implications for neurodegeneration, the predisposition of neurons to form FUS cytoplasmic inclusions, and the apparent lack of astrocytic pathology in FUS proteinopathies, including ALS-FUS (Mackenzie et al., 2011) and FTLD-FUS (this study).

RESULTS

Osmotic, but Not Oxidative, Stress Drives Cytoplasmic Translocation of Endogenous Neuronal FUS

To understand the involvement of cellular stress in the initiation of FUS pathology, we used mouse brain organotypic cortico-hippocampal slices, which are morphologically similar to the intact CNS (Figure S1A). We first tested the effect of hyperosmolar stress on SG formation and recruitment of FUS. Indeed, in cortical neurons, T-cell intracellular antigen-1 receptor (TIAR)-positive SGs were formed in the cytoplasm, most prominently at 4 hr of osmotic stress (Figure 1A). Moreover, nuclear FUS started to move into the cytoplasm at 2 hr, whereas at 4 hr of osmotic stress large amounts of FUS were redistributed, leading to partial nuclear clearance (Figures 1A and 1B). Cytoplasmic FUS was then colocalized with TIAR in a granular pattern indicating its association with SGs (Figures 1A and 1B). Interestingly, if osmotic pressure was applied continuously, cells adapted, SGs disassembled, and FUS relocalized to the nucleus, as early as 8 hr after stress initiation. Once adapted, cells survived with no observable signs of stress or FUS reaction for up to 7 days in hyperosmotic medium (Figure 1A). Quantification of cytoplasmic FUS in cortical neurons revealed a significant increase of up to 42% at 4 hr post-stress, compared with 12% in non-treated conditions, and reversal to pre-treatment levels by 8 hr (Figure 1C). This effect could also be validated in hippocampal neurons (Figure S1B). Despite this strong mislocalization, overall FUS protein levels were unaffected (Figure S1C) and its solubility to different detergents remained unchanged (Figure S1D).

To determine whether human neuronal FUS also reacts to hyperosmolar stress, we explored our recently established human neural stem cells (NSCs), which can be differentiated into mature neural cultures (data not shown). Indeed, in human neurons, nuclear FUS moved to the cytoplasm and neuronal processes, and colocalized with the SG marker protein G3BP (Ras GTPase-activating protein-binding protein) in a granular pattern (Figure 1D). A significant increase in cytoplasmic FUS, albeit without the nuclear clearance seen in mouse neurons, was detected already within 15 min of osmotic stress and intensified over a time course of 4–8 hr (Figure 1E). In contrast with mouse neurons in slice cultures, no complete recovery was seen in the human neuronal network upon continuous osmotic pressure. However, from 8 hr onward, several recovering neurons with relocalized nuclear FUS were observed, indicating the same principal mechanism of adaptation and recovery. However, some cells lost their morphological integrity, apparently unable to cope with cellular stress (Figure S1E). This varying adaptability was also reflected in the large variability observed in cytoplasmic FUS quantification at 96 hr (Figure 1E).

It was previously shown that FUS is recruited to SGs induced by oxidative stress (Andersson et al., 2008). However, in mouse brain slices, cytoplasmic SGs elicited by oxidative stress (OX) did not recruit FUS (Figure 1B). In only a minor subset of cells, very intense TIAR granules contained small amounts of FUS

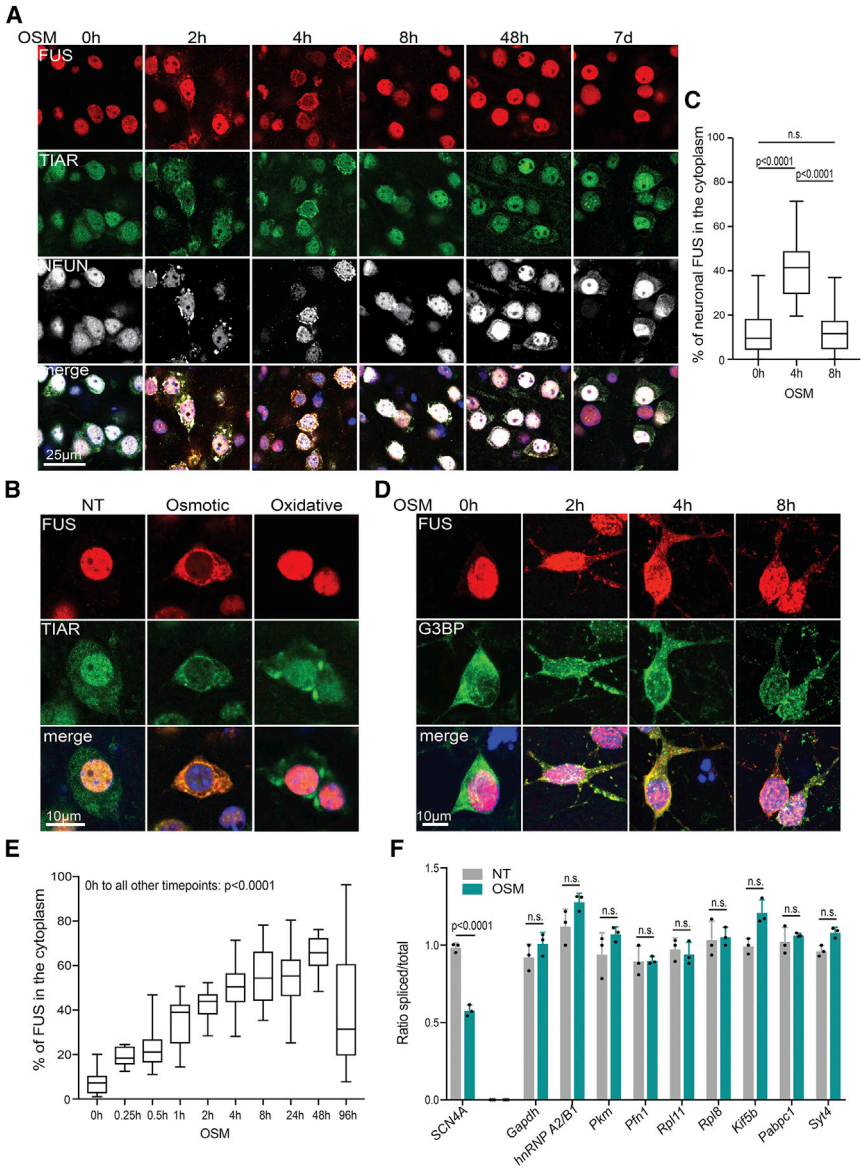


Figure 1. Osmotic, but Not Oxidative, Stress Drives Cytoplasmic Translocation of Endogenous Neuronal FUS

(A) Time course of hyperosmolar stress induced by 0.4 M sorbitol in mouse organotypic cortico-hippocampal brain slices. Nuclear FUS started to redistribute to the cytoplasm at 2 hr and reached a peak at 4 hr, when it colocalized with cytoplasmic SGs marked by TIAR. It dynamically relocalized to the nucleus within 8 hr, when TIAR granules were also resolved. FUS then stayed unaffected during a time course of 7 days of continuous stress.

(B) Osmotic stress elicited a distinct response of FUS, whereas oxidative stress could not sequester nuclear FUS into cytoplasmic TIAR-positive SGs induced by 0.5 mM arsenite.

(C) Quantification of neuronal FUS outside the nucleus showed the dynamic reaction of normally nuclear neuronal FUS, moving out to the cytoplasm at 4 hr and returning to the nucleus at 8 hr in mouse brain slices (n = 33–58 images from 6 independent experiments; data are represented as box and whisker plot).

(D) Time course of hyperosmolar stress in NSC-derived human neurons. Upon stress, FUS mislocalized to cytoplasmic granules, costained with the SG marker G3BP.

(E) Quantification of FUS outside the nucleus in human neuronal cultures across the hyperosmolar stress time course. A significant portion of FUS mislocalized to the cytoplasm already at 15 min of hyperosmotic stress (3 independent experiments, n = 10–30; data are represented as box and whisker plot).

(F) Osmotic stress led to splicing defects in the minigene *SCN4A* in NSC-34 cells as seen by the significantly decreased ratio of spliced to total target mRNA in qRT-PCR results at 2 hr of osmotic stress, whereas nine control mRNAs were not significantly affected (data are represented as mean with SD).

Merged images always include nuclear DAPI staining. NT, non-treated; OSM, hyperosmolar stress.

(Figure S1F). Confirming our observations in mouse brain slices, human neuronal FUS also showed a very distinct reaction to oxidative stress (Figure S1H), with most protein remaining nuclear, despite prominent cytoplasmic SGs (Figure S1G) and minor amounts of FUS rarely detected in large SGs (Figure S1G, arrow).

We verified that FUS redistribution is a general response to hyperosmolar stress using sucrose in brain slices (Figures S1I and S1J). Interestingly, no induction of SGs or FUS cytoplasmic translocation was seen using urea (Figure S1K), which is a neutral solute and can move freely in and out of cells without inducing hypertonic pressure. Similarly, hypoosmolar stress induced no visible shift of nuclear FUS (Figure S1L), indicating that the robust cytoplasmic redistribution of FUS is specific to hypertonic pressure.

Hyperosmolar Stress Leads to Loss of Nuclear FUS Function

Based on the drastic shift of FUS from its normal nuclear localization to the cytoplasm, we speculated that its nuclear function might be compromised under stress. To test this, we measured the splicing levels of *SCN4A* (sodium voltage-gated channel alpha subunit 4), a minor intron-containing transcript that is directly regulated by FUS (Reber et al., 2016). In motor neuron-like NSC-34 cells, we observed a strong reduction of spliced-to-total *SCN4A* ratios during osmotic stress with no change of FUS levels (Figures 1F, S1M, and S1N). This observation resembles the effect seen after FUS knockdown or cytoplasmic mislocalization due to ALS-associated mutations in NLS (Reber et al., 2016). In contrast, nine control mRNAs, whose splicing is FUS independent (Reber et al., 2016), displayed no significant

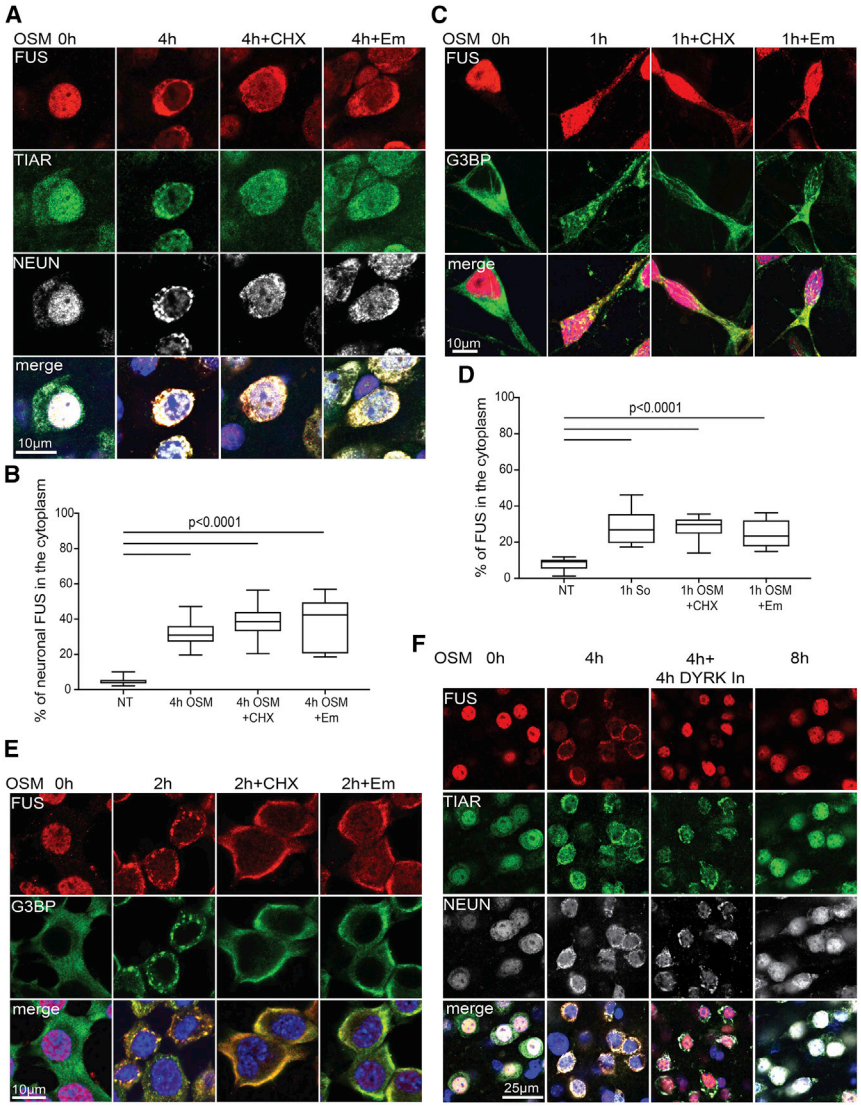


Figure 2. Cytoplasmic Translocation of FUS Is Independent of Stress Granule Formation

(A) FUS redistribution to the cytoplasm with partial nuclear clearance caused by osmotic stress was not reversed by SG inhibitors (CHX, Em) in neurons within mouse brain slices. Upon SG inhibition, both FUS and TIAR showed a diffused pattern, indicating the successful prevention of SG formation.

(B) Quantification of cytoplasmic FUS in neurons confirmed significant mislocalization also during SG inhibition (n = 18–25; data are represented as box and whisker plot).

(C) No change of FUS behavior upon osmotic stress was seen in human neurons when SG formation was blocked.

(D) Quantification of human FUS outside of the nucleus confirms significant redistribution also during SG inhibition (n = 10; data are represented as box and whisker plot).

(E) Diffuse cytoplasmic FUS localization upon SG inhibition was especially obvious in NSC-34 cells in comparison with distinct SGs labeled by G3BP in the absence of SG inhibitors.

(F) Although treatment with a DYRK inhibitor (GSK-626616) for 4 hr at the peak of osmotic stress stabilized TIAR-positive SGs in mouse slice cultures, FUS escaped these and returned to the nucleus with unchanged kinetics.

Merged images always include nuclear DAPI staining. In, inhibitor; NT, non-treated; OSM, hyperosmolar stress.

splicing alterations upon osmotic stress, indicating a functional impairment of FUS during osmotic stress.

Cytoplasmic Translocation of FUS Is Independent of Stress Granule Formation

To understand the molecular mechanism of this cytoplasmic translocation during osmotic stress, we tested whether SG formation was necessary to sequester FUS to the cytoplasm. Thus, we treated organotypic slices and human neurons with cycloheximide (CHX) and emetine (Em), which are translational inhibitors known to block SG formation (Kedersha et al., 2000). After excluding that CHX or Em alone altered FUS localization (Figure S2A), we verified that both reagents inhibit SGs (Figure S2B) and block protein synthesis (Figure S2C). Surprisingly, neither treatment reversed the robust cytoplasmic localization of FUS (Figures 2A–2D), which was diffusely distributed to the cytoplasm in the absence of SGs (Figures 2A, 2C, and 2E).

In line with these observations, SG stabilization with a DYRK inhibitor (dual-specificity tyrosine-regulated kinase, GSK-626616), which was previously shown to prevent SG disassembly (Wippich et al., 2013), did not prolong cytoplasmic FUS localization. Even though GSK-626616 treatment stabilized TIAR-positive SGs for an additional 4 hr, FUS escaped these structures and relocated to the nucleus with kinetics similar to cells treated only with sorbitol (Figure 2F). Collectively, these data indicate that cytoplasmic FUS redistribution in hyperosmolar conditions is SG independent, and that dynamic FUS nucleocytoplasmic shuttling is unaffected by alterations in SG kinetics.

FUS Redistribution to the Cytoplasm Is Independent from Hyperosmolar Stress Pathways

Osmotic shock is known to activate the three main mitogen-activated protein kinase (MAPK) signaling pathways involving p38, extracellular-signal-regulated kinase (ERK), and c-Jun N-terminal kinase (JNK), and others including Src family kinases Fyn and Syk, as well as protein kinase C (PKC) (Sheikh-Hamad and Gustin, 2004). In agreement with this, we confirmed the activation of MAPK cascades upon hyperosmotic treatment in mouse brain slices, human neurons, and NSC-34 cells (Figures S3A–S3C). To test their potential role in FUS subcellular redistribution during osmotic stress, we used a panel of pharmacological

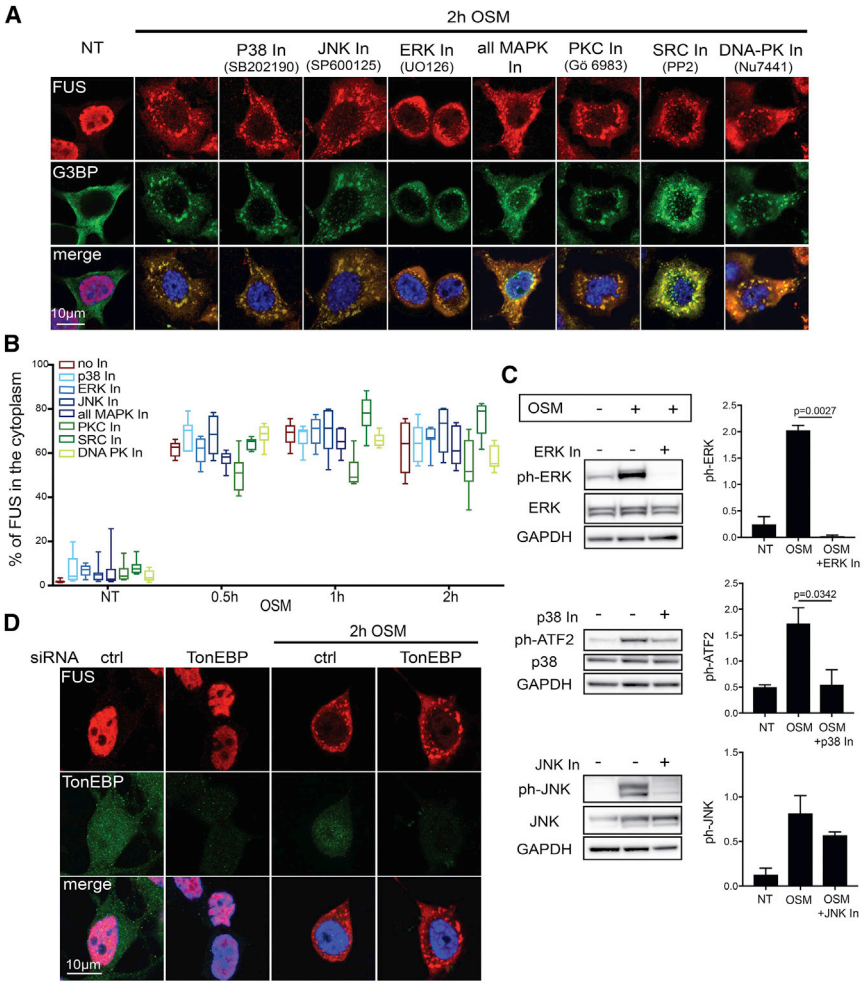


Figure 3. FUS Redistribution to the Cytoplasm Is Independent from Hyperosmolar Stress Pathways

(A and B) Treatment of NSC-34 cells with inhibitors of stress-activated kinases and pathways did not interfere with stress-induced FUS mislocalization, shown in representative images at 2 hr OSM (A) and quantification of FUS outside the nucleus during the stress time course (B) (n = 7–10, data are represented as box and whisker plot). No significant reduction was observed in any of the conditions tested except the early time points of PKC inhibition (30 min: p = 0.0083, 1 hr: p = 0.0005), whereas rather increased amounts of cytoplasmic FUS were observed upon SRC inhibition (1 hr: p = 0.0285, 2 hr: 0.0229) and DNA PK inhibition at 30 min (p = 0.0103).

(C) Inhibition of the main MAPK by their respective inhibitors (ERK by UO126, p38 by SB202190, JNK by SP600125) was confirmed by immunoblots for phosphorylated forms or ERK and JNK (ph-ERK and ph-JNK, respectively) or phosphorylation of a downstream p38 target (ph-ATF2), whereas their levels did not change. Representative immunoblots and average of the densitometry quantification of three replicates are plotted with SEM.

(D) Reduction of the master osmoregulator TonEBP by siRNA did not alter FUS cytoplasmic redistribution upon stress.

Merged images always include nuclear DAPI staining. ctrl, control; In, inhibitor; NT, non-treated; OSM, hyperosmolar stress.

inhibitors. Inhibition of ERK1/2, p38, and JNK was confirmed by decreased phosphorylation either of the kinases themselves or their respective targets. Nevertheless, this inhibition did not prevent cytoplasmic FUS accumulation during stress (Figures 3A–3C). Similarly, inhibiting Src-family kinases or PKC did not reduce sorbitol-induced FUS relocalization at 2 hr of osmotic stress, whereas a slight decrease in cytoplasmic FUS was seen upon PKC inhibition at 30 min and 1 hr. Osmotic stress was also reported to trigger DNA damage (Dmitrieva et al., 2004; Kültz and Chakravarty, 2001), which in turn leads to FUS nuclear exit, a process controlled by its phosphorylation by DNA-dependent protein kinase (DNA-PK) (Deng et al., 2014). However, whereas FUS remains nuclear when DNA-PK is inhibited upon staurosporine treatment (Figure S3D), no effect on sorbitol-induced mislocalization was observed by DNA-PK inhibition (Figures 3A and 3B).

A major mediator of the osmotic stress response is the transcription factor TonEBP (tonicity response element binding protein), whose activation induces the expression of osmoprotective target genes. Although we observed activation of TonEBP by its nuclear translocation in osmotic conditions, no change was observed on FUS cytoplasmic mislocalization after downregulation of TonEBP by small interfering RNA (siRNA) (Figure 3D). Our results indicate that FUS redistribution is independent of the major signaling pathways activated by hyperosmolar stress.

FUS Leaves the Nucleus by Passive Diffusion upon Osmotic Stress

To decipher the underlying mechanism for FUS redistribution during osmotic stress, we next investigated its nuclear exit route, including receptor-mediated transport, in complex with mRNA or passive diffusion. Because a CRM1/Exportin-1-dependent leucine-rich nuclear export signal has been predicted within the FUS RNA recognition motif (RRM) domain, we first tested whether this export factor is active during hyperosmolar stress. We found that FUS redistribution was not prevented by leptomycin B (LMB) (Figures 4A and 4B), although CRM1 effectively inhibited shuttling of its known targets p62 and REV (Kudo et al., 1999; Pankiv et al., 2010) (Figures S4A and S4B). This indicated that FUS leaves the nucleus independently of CRM1-mediated export during sorbitol-induced stress.

Second, we tested whether FUS utilizes the mRNA export machinery to exit the nucleus by silencing Aly/REF, an essential factor of the TREX (transcription-export) complex, necessary for

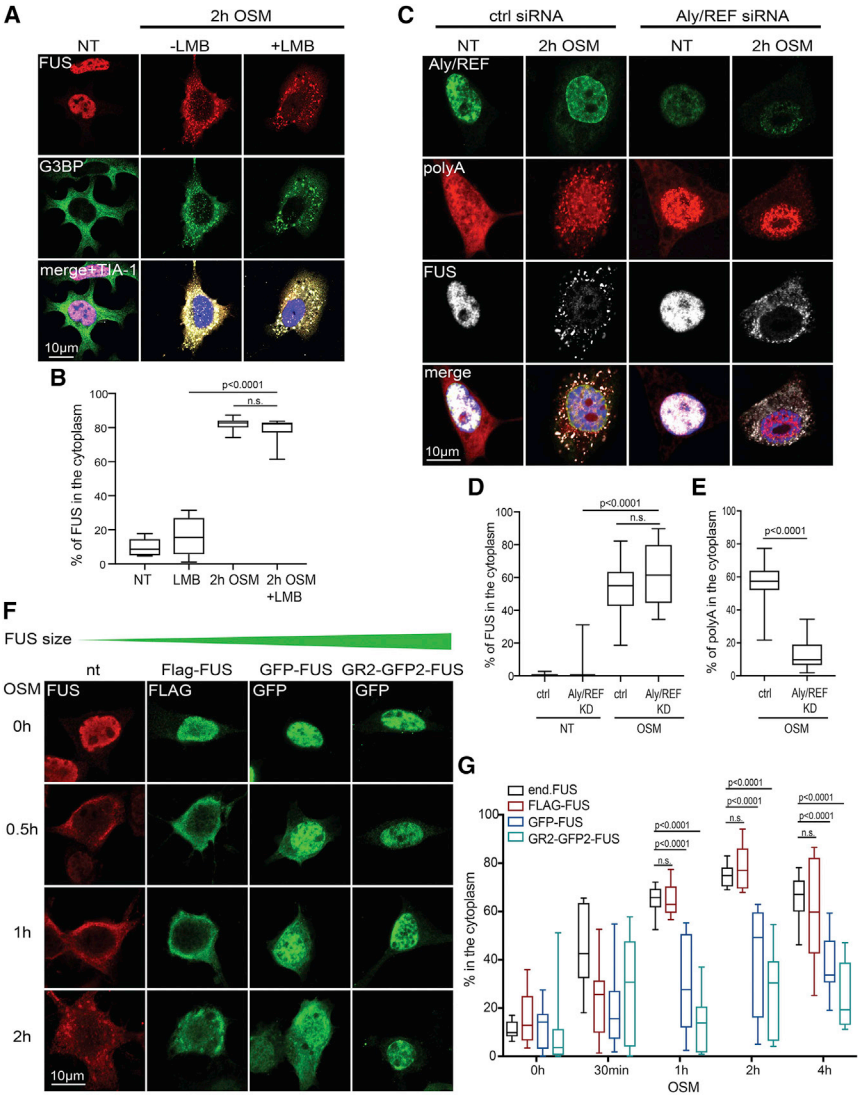


Figure 4. FUS Leaves the Nucleus by Passive Diffusion upon Osmotic Stress

(A and B) Inhibition of CRM1/Exportin1 by leptomycin B (LMB) in NSC-34 cells did not prevent FUS cytoplasmic localization upon osmotic stress, shown in representative images (A) and quantification of FUS outside the nucleus (B) (n = 7–8 images, data are represented as box and whisker plot).

(C) Despite mRNA retention in the nucleus, caused by siRNA-mediated knockdown of the mRNA export complex factor Aly/Ref, FUS accumulated in the cytoplasm upon osmotic stress.

(D–G) Quantification of FUS outside the nucleus (D) was performed in single cells with retained nuclear polyA mRNA as confirmed in (E) (n = 11–17 images, data are represented as box and whisker plot).

(F–G) NSC-34 cells transfected with artificially enlarged FUS constructs displayed a size-dependent restriction of FUS movement across the nuclear membrane in osmotic stress. Addition of sorbitol led to cytoplasmic mislocalization of endogenous and FLAG-tagged FUS in their standard time frame, whereas GFP-FUS and GR_2-GFP_2-FUS showed delayed export kinetics, depending on their respective size as seen in representative images (F) and quantification of different FUS constructs outside the nucleus (G) (n = 9–11 images, data are represented as box and whisker plot).

Merged images always include nuclear DAPI staining. nt, non-transfected; NT, non-treated; OSM, hyperosmolar stress.

transporting mRNAs through the nuclear pore complex (NPC) (Katahira, 2012; Sloan et al., 2016). Accumulation of polyA mRNA in nuclei upon decreased Aly/REF expression confirmed inhibition of mRNA export (Figures 4C and 4E), but did not result in nuclear retention of FUS when osmotic stress was applied in parallel (Figures 4C and 4D). Hence, hyperosmolarity-induced FUS mislocalization did not depend on functional mRNA export.

Lastly, we tested whether passive diffusion could be the main exit mechanism. We hypothesized that increasing the size of FUS would decrease its movement through the nuclear pores, because passive diffusion rate is mainly dependent on molecular mass (Timney et al., 2016). To test this, we used a combination of differently sized FUS constructs, apart from endogenous FUS, including FLAG-tagged FUS (FLAG-FUS; 54.5 kDa), single EGFP-tagged FUS (GFP-FUS; 90 kDa), and a fusion FUS protein containing two glucocorticoid receptor (GR) hormone-binding domains coupled with two EGFPs (GR_2-GFP_2-FUS; 172 kDa). Even though FLAG-FUS could exit the nucleus with kinetics similar to the endogenous protein, significantly reduced amounts of GFP-FUS were found in the cytoplasm (Figures 4F and 4G). Although the initially cytosolic GR_2-GFP_2-FUS rapidly translocated into the nucleus upon dexamethasone addition (Figure S4C) (Ederle et al., 2018), its artificial size increase almost completely prevented its exit during stress, whereas endogenous FUS was redistributed to the cytoplasm in the same cells (Figure S4D). Our enlarged version of the CRM1 cargo protein REV (GR-GFP-REV) confirmed that active receptor-mediated export was not altered under these conditions (Figure S4C). Collectively, these data indicate that FUS leaves the nucleus by passive diffusion under osmotic conditions, in line with the mechanism used under physiological conditions (Ederle et al., 2018).

Osmotic Stress-Induced FUS Redistribution Is Potentiated by Transcriptional Inhibition

The primarily nuclear FUS localization under physiological conditions (Figure 1A) implies that steady-state nuclear import is higher than export. The large amounts of cytoplasmic FUS observed under osmotic stress therefore indicate either increased exit or decreased nuclear import. Augmented egress out of the nucleus can be explained by higher diffusion rate across the nuclear membrane, which is limited by macromolecular size, suggesting

that FUS partitioning in higher-molecular-weight nuclear complexes may favor its nuclear localization (Wühr et al., 2015). Indeed, FUS was shown to bind numerous pre-mRNAs (Lagier-Tourenne et al., 2012) and to interact with RNA polymerase II (Pol II) (Bertolotti et al., 1996, 1998; Schwartz et al., 2012) and splicing complexes in the nucleus.

In line with known effects during osmotic stress (Finan and Guilak, 2010), we observed alterations in DNA and nuclear speckle organization (Figures S5A and S5B). Such stress-induced rearrangements may abolish some nuclear interactions of FUS and lead to more free FUS able to diffuse out of the nucleus. Indeed, some studies have found a slight redistribution of FUS into the cytoplasm (Zinszner et al., 1994) and loss of nuclear FUS foci upon actinomycin D (ActD) treatment (Patel et al., 2015). ActD inhibits transcription by interfering with Pol II progression (Trask and Muller, 1988), leading to a reduced supply of newly synthesized mRNA transcripts, which in combination with possible disruption of larger transcription and splicing complexes might increase FUS diffusion. To test this, we treated cells with ActD with or without hyperosmolar stress. Although we could not detect a cytoplasmic shift in human neurons upon ActD treatment alone, combination of ActD with osmotic stress led to a strong synergistic effect with significant increase in cytoplasmic FUS, compared with solely osmotic stress (Figure 5A). Interestingly, in NSC-34 cells we detected some cytoplasmic FUS upon transcriptional inhibition alone, either by ActD (Figure S5C) or as an inhibitor selectively targeting Pol II (DRB) (Figure S5D), as described before (Kino et al., 2011; Zinszner et al., 1994). This finding indicates that decreased possibilities for RNA binding and complex formation in the nucleus might increase FUS diffusion through nuclear pores, even in the absence of stress. Yet, hyperosmolar pressure strongly amplifies this effect in neurons and NSC-34 cells.

Cytoplasmic Translocation of FUS upon Hypertonic Pressure Results from Insufficient Import by TNPO

A shift in FUS subcellular distribution might also be caused by insufficient nuclear import, which is effectively executed by TNPO (Dormann et al., 2010; Lee et al., 2006). To test a potential TNPO import defect, we monitored its cargo proteins hnRNPA1 (heterogeneous nuclear RNP A1), TAF15, and EWS upon hyperosmolar stress and confirmed their cytoplasmic shift in mouse brain slices (Figures 5B and 5C) and human neurons (Figure 5D). The same effect was detected for all other tested TNPO cargo proteins, including SAM68 (Figure S5E) and hnRNPA2B1 (Figure S5F), as well as the neuronal marker NEUN (Figure 1A), which also contains a PY-NLS (Dredge and Jensen, 2011). To exclude that sorbitol induces a general leakage of the nuclear membrane, we verified that the non-shuttling protein heterogeneous nuclear ribonucleoprotein U (hnRNPU) retained its nuclear localization upon osmotic stress (Figure S5G). We then wondered whether other shuttling proteins employing different import receptors were also affected. The functionally related, ALS-associated protein TDP-43, which uses a classical NLS recognized by importin α/β (Dormann and Haass, 2011), did not translocate to the cytoplasm upon osmotic stress in brain slices (Figure 5E) or human neurons (Figure 5D). Similarly, the importin α/β cargo p53 (Liang and Clarke, 1999) accumulated in nuclear patches upon sorbitol treatment (Figure S5H), as previously described (Nakaya et al., 2009). These findings indicate that hyperosmolar stress did not impair all transport through the nuclear pore, but specifically TNPO-mediated nuclear import.

Due to the specificity of this stress response, we then monitored TNPO expression and localization during hyperosmolar stress. Although protein levels did not change (Figure S5I), its subcellular localization was altered (Figure 5F). TNPO was dispersed throughout the cytoplasm and the nucleoplasm under physiological conditions, while upon osmotic pressure it displayed a significant shift toward the cytoplasm in a manner that correlated with FUS redistribution in neurons (Figures 5F and 5G), as well as NSC-34 cells (Figures S5J–S5M). In the cytoplasm TNPO1 localized to SGs together with FUS and the SG marker eIF3η (eukaryotic initiation factor 3); however, inhibiting SG formation did not prevent the cytoplasmic shift of TNPO1 (Figure S5K). This response was specific for TNPO, because Importin 7, which is normally dispersed in the nucleus and cytoplasm, did not show a change in subcellular localization (Figures S5L and S5M).

We next asked whether increased TNPO levels could rescue the sorbitol-induced FUS relocalization. Interestingly, overexpressing HA-tagged TNPO1 in NSC-34 cells led to two distinct cell populations with a differing reaction to osmotic stress. Although in some cells HA-TNPO1 was detained in the cytoplasm upon stress like its endogenous counterpart, in a subpopulation of cells HA-TNPO1 localized largely to the nucleus and was able to cause a clear recovery of nuclear FUS localization (Figure 5H).

Taken together, based on the specificity of the cargo mislocalization and its rescue by nuclear TNPO, we hypothesize that TNPO cytosolic retention contributed to redistribution of FUS and other cargos. Overall, the observed hyperosmolar stress response mimics a loss of TNPO function, as previously described (Dormann et al., 2010). Upon osmotic stress, this specific TNPO and cargo exclusion from the nucleus might represent a physiological stress response.

Astrocytes Are Spared from Stress-Induced Cytoplasmic Translocation of FUS

One advantage of organotypic slice cultures is the presence and interplay of all different cell types found in the CNS. During our initial osmotic stress experiments we noticed that, although reacting cells showed a very strong FUS mislocalization, certain cells did not respond at all. Using cell-type-specific markers during the stress time course, we confirmed a strong and dynamic FUS redistribution in all neurons (Figure 1A), as well as in microglia (Figures 6A and S6A). Notably, the neuronal marker NEUN, which is also an RBP involved in splicing (Kim et al., 2009), formed a similar granular pattern during stress (Figure 1A), suggesting that it is sequestered in SGs. In contrast, astrocytes identified by GFAP (glial fibrillary acidic protein) remained unaltered during 8 hr of continuous stress, while surrounding GFAP-negative cells reacted strongly (Figures 6B and S6B). To test whether human astrocytic FUS is similarly non-reactive to hyperosmolar stress, we used distinct neuronal and astrocytic cultures derived from our human NSCs. Intriguingly, human

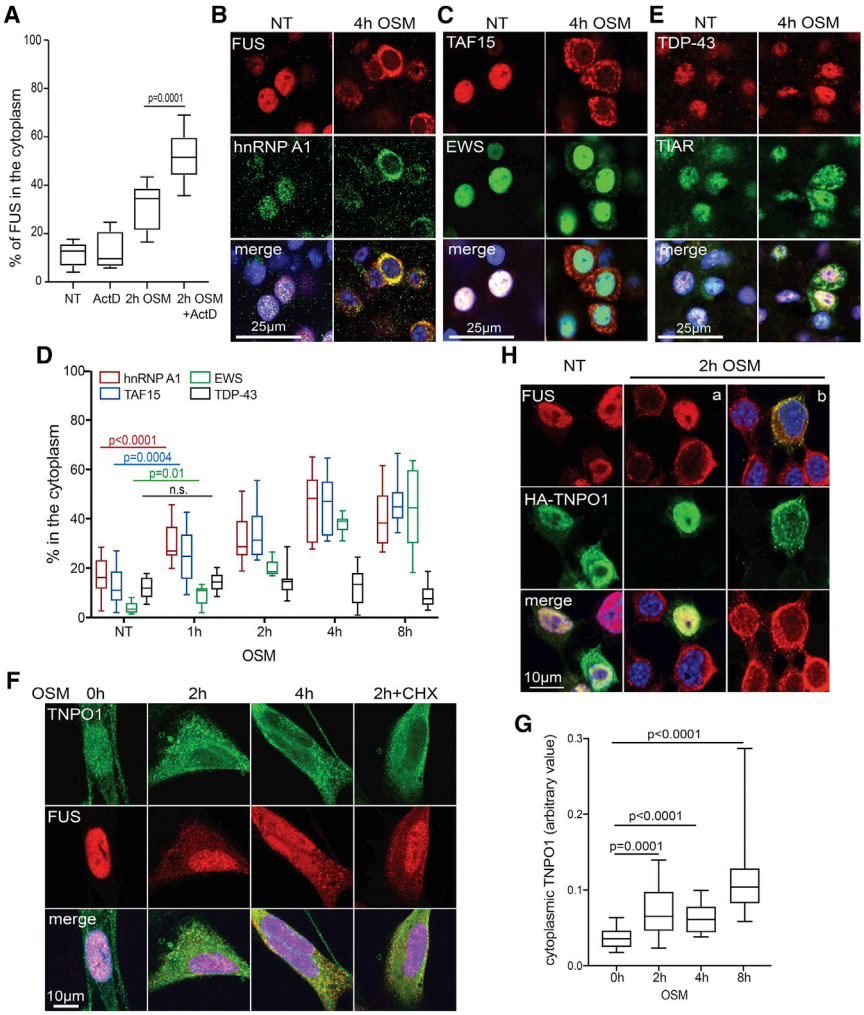


Figure 5. Osmotic Stress-Induced FUS Redistribution Is Potentiated by Transcriptional Inhibition and Results from Insufficient Import by TNPO

(A) Quantification of FUS outside the nucleus in human neurons revealed the synergistic effect of transcriptional inhibition by ActD and osmotic pressure compared with either factor alone (n = 10 images; data are represented as box and whisker plot).

(B) hnRNPA1 displayed a dynamic reaction similar to FUS during osmotic stress in neurons in mouse brain slices.

(C) TAF15 strongly localized to the cytoplasm upon osmotic stress in neurons of mouse brain slices, whereas EWS mislocalized to a lesser extent.

(D) Quantification of cytoplasmic protein levels in human neurons confirmed the mislocalization of hnRNPA1, TAF15, and EWS (n = 10–15 images), but not TDP-43, upon osmotic stress (n = 13–15 images; data are represented as box and whisker plot).

(E) TDP-43 did not shift to the cytoplasm upon osmotic stress, whereas TIAR-positive SGs were formed.

(F) TNPO1 nucleocytoplasmic equilibrium shifted toward the cytoplasm upon osmotic stress in human neurons, correlating with cytoplasmic FUS mislocalization.

(G) Quantification of cytoplasmic TNPO1 in human neurons confirmed a significant shift upon osmotic stress (n = 18–20 images; data are represented as box and whisker plot).

(H) Overexpression of HA-tagged TNPO rescued FUS mislocalization, when TNPO could shuttle to the nucleus (a), whereas surrounding non-transfected cells showed the standard osmotic stress-induced response. In a subpopulation of transfected cells, HA-tagged TNPO1 was retained in the cytoplasm (b) and did not rescue FUS localization. Merged images always include nuclear DAPI staining. NT, non-treated; OSM, hyperosmolar stress.

astrocytes were non-reactive to this insult, because FUS remained nuclear in both pure astrocytic cultures (Figure 6C) and astrocytes found within the neural network (Figure S6C). This resistance to osmotic stress was maintained over a period of multiple days and represents a distinct reaction compared with neuronal FUS (Figure 6D). In line with the observation in neurons, FUS was not sequestered into the cytosol because of oxidative stress in astrocytic cultures, despite the formation of bona fide SGs labeled with G3BP and eIF3η (Figure S6D).

Despite Their Reaction to Hyperosmolarity, Astrocytes Do Not Show This TNPO-Specific Stress Response

Because neurons and astrocytes were derived from the same human NSCs, we tested whether these progenitor cells show sensitivity to osmotic stress and if so, at which time point in differentiation cells with astrocytic fate lose their sensitivity. Undifferentiated NSCs showed a strong sensitivity to osmotic stress, and FUS was driven to the cytoplasm in cells labeled by the stem cell marker SOX2 (sex determining region Y, box 2) and low levels of MAP2/NEFM (microtubule-associated protein 2/neurofilament medium polypeptide). Interestingly, only 3 days into differentiation, a subpopulation of cells with slightly larger nuclei exhibited decreased reactivity to osmotic stress. These cells had lost SOX2 and the neuronal markers MAP2/NEFM, and showed an altered VIM (vimentin) pattern, which is highly expressed in astrocytes, indicating that they might be committed toward an astrocytic cell fate (Figures S6E and S6F).

Interestingly, activation of stress-signaling cascades (Figure 7A) and alterations in nuclear architecture (Figures 7B and S7A) were detected in astrocytes upon osmotic stress similarly to neurons. We next asked whether differences in FUS import could explain the distinction. We confirmed that TNPO is the responsible shuttling factor in astrocytes, because its inhibition led to increased amounts of FUS in the cytosol (Figure 7C), whereas blocking importin α/β did not (Figure S7B). This finding, in conjunction with our observation that nuclear TNPO overexpression reduced FUS mislocalization (Figure 5H), raised the possibility that astrocytes might express higher TNPO levels, thereby efficiently transporting FUS to the nucleus, even under osmotic stress. However, when comparing TNPO levels of astrocytes with a panel of reacting cell types, we did not detect an increase in astrocytic TNPO 1 or 2 (Figure S7C). Moreover,

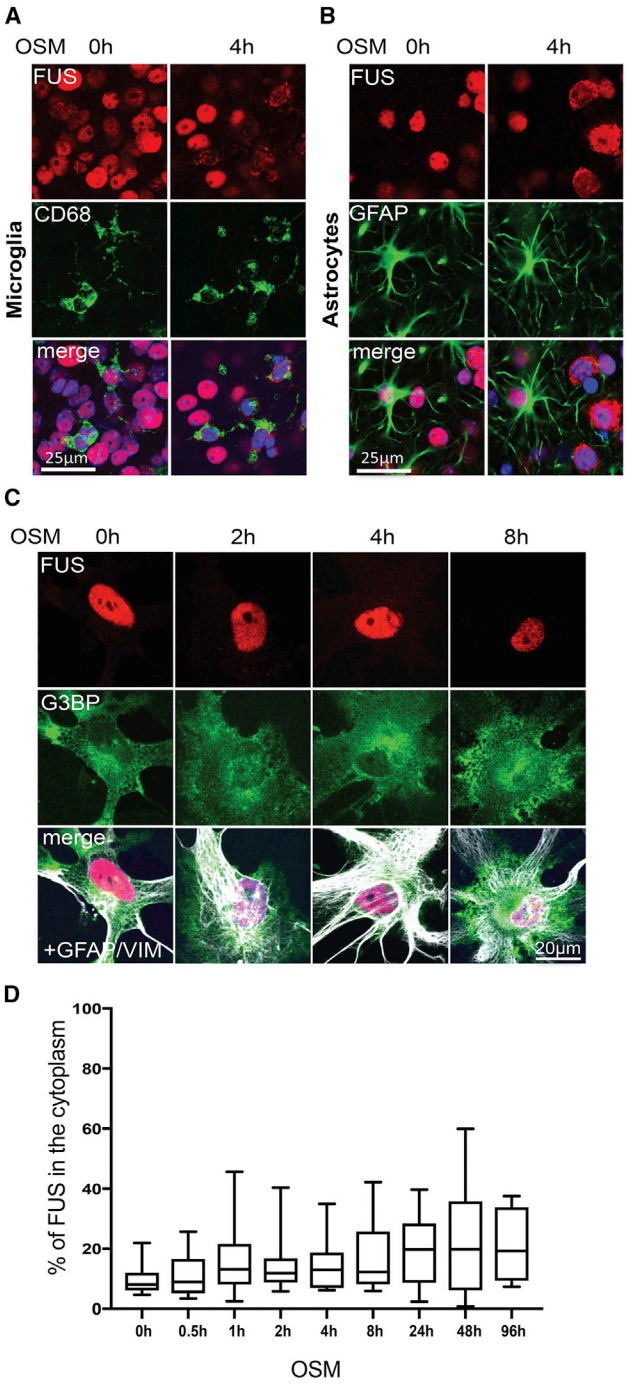


Figure 6. Astrocytes Are Spared from Stress-Induced Cytoplasmic Translocation of FUS

(A and B) In mouse brain slices FUS redistribution due to sorbitol treatment was observed in CD68-positive microglial cells (A), whereas it stayed nuclear in mouse GFAP-positive astrocytes (B).

(C) Pure human NSC-derived astrocyte cultures, labeled with the astrocyte markers VIM and GFAP, did not show FUS cytoplasmic redistribution upon osmotic stress.

(D) Quantification of non-nuclear FUS in human astrocytes confirmed their non-reactivity to hyperosmolar stress (n = 8–15; data are represented as box and whisker plot).

monitoring TNPO levels during osmotic stress did not reveal an increase of TNPO in astrocytes (Figure S7D).

Intriguingly, when monitoring the subcellular localization of TNPO upon osmotic stress in pure astrocyte cultures, we did not detect a cytoplasmic shift (Figures 7D, 7E, S7E), as seen in neurons and other reacting cells. The correlation between TNPO localization and FUS redistribution was further confirmed comparing FUS reactive and non-reactive cells with normal or altered TNPO localization, respectively, in mixed neuronal and astrocytic cultures (Figure S7F). Together with the observation that only nuclear, and thus supposedly shuttling, TNPO rescued FUS redistribution (Figure 5H), we postulate that cytoplasmic retention of TNPO impairs its import function, and that this specific hyperosmolar stress response is not implemented in astrocytes.

It was previously reported that astrocytes are spared from pathological findings in ALS patients with FUS mutations (Mackenzie et al., 2011), so we wondered whether that might also be true for FTLD-FUS, in which TNPO1 was found to coaggregate in FUS-positive inclusions. TNPO1 immunostaining of FTLD-FUS post-mortem tissue showed numerous neuronal cytoplasmic inclusions, intranuclear inclusions, and neuropil threads in the frontal cortex as previously observed (Brelstaff et al., 2011). Intriguingly, double immunostaining with GFAP showed no colocalization between TNPO1 pathological inclusions and reactive astrocytes in FTLD-FUS (Figures 7F and S7G).

DISCUSSION

The RPB FUS marks pathological cytoplasmic inclusions in distinct subtypes of ALS and FTD with early disease onset. Although FUS can shuttle between the nucleus and the cytoplasm, its physiological steady state is predominantly nuclear. This equilibrium is maintained by constant nuclear import through TNPO, but can be shifted to the cytosol either by inhibition of this shuttling receptor (Dormann et al., 2010) or genetic disruption of its NLS by ALS-causing mutations (Kwiatkowski et al., 2009; Vance et al., 2009). Because FTD-FUS cases show no underlying mutations, we tested the stress-induced nucleocytoplasmic shuttling of endogenous FUS in an *ex vivo* mouse CNS model and human neural networks. We identified hyperosmolar stress as a robust driver of cytoplasmic translocation of wild-type FUS and other cargos of TNPO in neurons. This diffusion-based reaction was independent of SG formation and classical osmoregulatory pathways, and was potentiated by transcriptional inhibition. Importantly, this specific response was mediated by cytoplasmic accumulation and impaired shuttling of TNPO, but not other transporting factors, and was surprisingly absent in astrocytes, which lack pathological TNPO accumulations in FTLD-FUS patient brains.

Cytoplasmic Translocation and Stress Granule Incorporation of FUS Are Uncoupled

Recruitment of FUS to SG resulting from a variety of stressors has been widely demonstrated, albeit most studies used

Merged images always include nuclear DAPI staining. OSM, hyperosmolar stress.

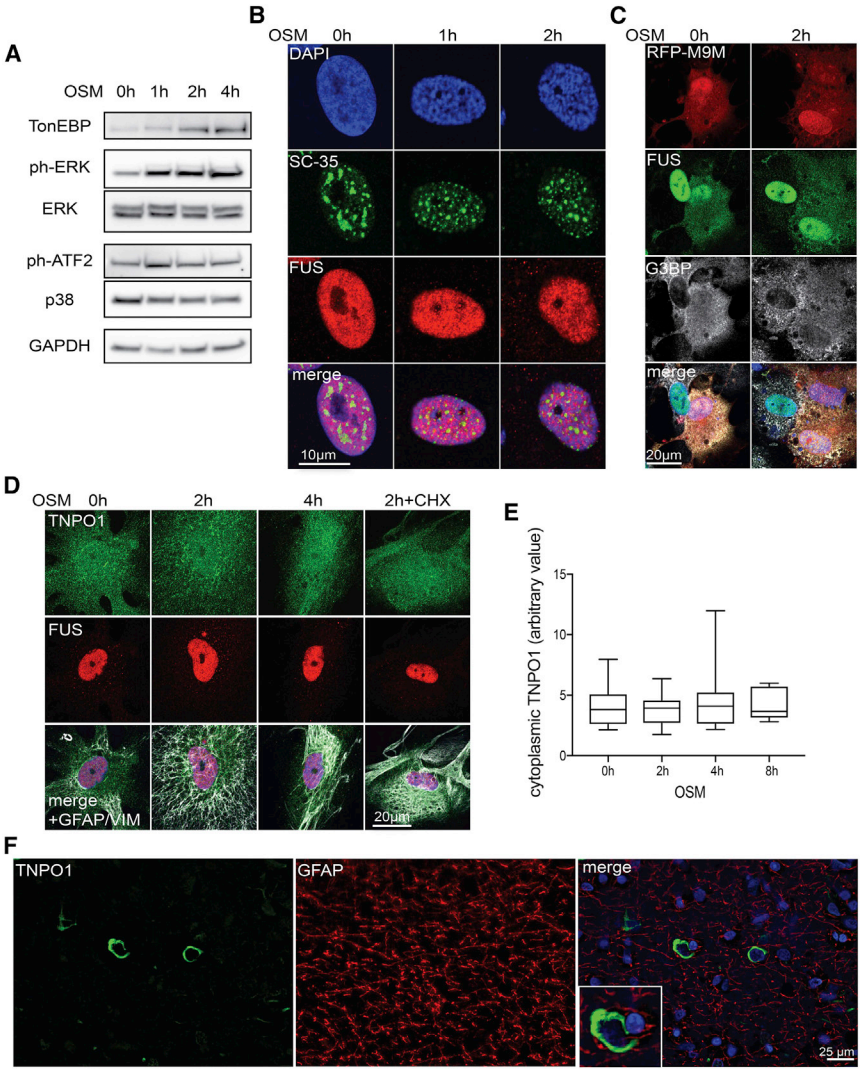


Figure 7. Despite Their Reaction to Hyperosmolarity, Astrocytes Do Not Show This TNPO-Specific Stress Response

(A) Immunoblots of TonEBP, ph-ERK, and ph-ATF2 confirmed the activation of general stress signaling cascades in human astrocytes compared with GAPDH and non-phosphorylated kinases (ERK, p38).

(B) Hyperosmolarity-induced nuclear rearrangement in human astrocytes, as observed by alterations in DNA (DAPI) and nuclear splicing speckles (SC-35) pattern.

(C) In human astrocytes expressing the RFP-tagged peptide inhibitor M9M (C), TNPO1 was blocked and FUS was shifted to the cytoplasm due to impaired nuclear import.

(D–E) TNPO1 subcellular distribution and nuclear FUS localization were unchanged upon osmotic stress in human astrocytes, shown in representative images (D) (merge with nuclear DAPI staining and astrocytic markers GFAP and VIM) and quantification of cytoplasmic TNPO1 (E) (n = 18–20 images, data are represented as box and whisker plot).

(F) Representative images of immunohistochemical staining of FTLD-FUS post-mortem human brain tissue. TNPO1-positive neuronal cytoplasmic inclusions were observed in the frontal cortex of a FTLD-FUS case, and GFAP immunohistochemistry showed an extensive network of reactive astrocytes and astrocytic processes. No TNPO1 immunoreactivity colocalized with GFAP-positive astrocytes.

OSM, hyperosmolar stress.

overexpression of the wild-type or NLS mutant protein (Anderson and Kedersha, 2009; Bentmann et al., 2012; Bosco et al., 2010; Vance et al., 2013). In our study, we focused on endogenously expressed FUS within differentiated neurons in their natural microenvironment and show that nuclear FUS is unaffected by cytoplasmic SG formation induced by arsenite.

Hyperosmolarity was recently reported to drive endogenous, nuclear FUS to cytoplasmic SGs, which were hypothesized to actively sequester endogenous FUS out of the nucleus to specifically localize certain mRNAs and proteins into these structures (Sama et al., 2013). In contrast, we found that FUS cytoplasmic localization was unaffected by inhibition of SG formation (Figures 2 and S2). This surprising finding indicates that SGs are not the driving factor pulling nuclear FUS into the cytoplasm. Supporting this, prolongation of cytoplasmic SGs could not retain endogenous FUS, which escapes these stabilized SGs to return to the nucleus in its own timeline of stress reaction (Figure 2F). Our data demonstrate that cytoplasmic translocation and SG partitioning of FUS are two independent processes, and that the former precedes the latter. Importantly, hyperosmolar stress incites both cytoplasmic FUS relocation and formation of TIAR/G3BP-positive granules, into which redistributed FUS is incorporated.

TNPO as a Stress Response Sensor or a Cytoplasmic Chaperone?

When dealing with sudden stress, cells utilize a wide range of mechanisms to temporarily block metabolic processes, including DNA replication, transcription, mRNA export, and translation. At the same time, they initiate stress-defense mechanisms via transcriptional activation, alternative splicing, and translational surge of stress response proteins. This binary response requires ways to selectively shut down or activate single factors or groups of functionally related proteins. On a translational level this task is performed by SGs, which selectively recruit cytoplasmic mRNAs and RBPs. Regulation of nuclear processes is achieved by changes in subcellular distribution and altered association with multiprotein complexes of many

splicing and transcription factors. The observed stress-induced shift of FUS to the cytoplasm and the concomitant decrease in its nuclear abundance are accompanied by loss of nuclear function (Figures 1F, S1M, and S1N), comparable with *FUS* knockdown (Reber et al., 2016). Moreover, the dynamic redistribution upon osmotic stress is shared by many, if not all, PY-NLS-containing proteins and correlates with the cytoplasmic shift of TNPO. Intriguingly, most experimentally validated PY-NLS-containing cargos are RBPs, whereas about 60% of proteins with predicted PY-NLS are involved in RNA transcription or processing (Lee et al., 2006). We thus propose that the subcellular redistribution of nuclear RBPs could act as a specific response to hypertonic pressure, caused by the cytoplasmic retention of TNPO.

Moreover, the increased cytoplasmic localization of TNPO might be a protective mechanism to counteract aberrant phase transitions of FUS and other aggregation-prone TNPO1 cargoes during stress. Indeed, several recent studies showed that nuclear import receptors, including TNPO1, function as cytoplasmic chaperones to prevent aberrant phase transitions of aggregation-prone RBPs with prion-like domains (Guo et al., 2018; Hofweber et al., 2018; Qamar et al., 2018; Yoshizawa et al., 2018). Aberrant phase transitions of such proteins may be favored because of macromolecular crowding during osmotic stress (Bounedjah et al., 2012), necessitating elevated levels of TNPO1 in the cytoplasm under these conditions.

Astrocytic Resistance to TNPO-Specific Stress Response

Here, we report the unique and surprising unresponsiveness of mouse and human astrocytes to osmotic stress, despite the comparable activation of stress cascades and no differences in their osmotolerance toward nuclear rearrangement. In contrast, we identified a striking divergence in the reaction of astrocytic TNPO and FUS upon hyperosmolarity (Figures 6, 7, S6, and S7). Astrocytes as one of the most resistant cell types in the brain express unique water channels called aquaporins (AQP) that allow passive water flux across their cell membrane (Risher et al., 2009). Indeed, AQP4 and AQP9 are upregulated upon hyperosmolarity in astrocytes through activation of MAPK- and TonEBP-mediated pathways (Arima et al., 2003; Yi et al., 2013), thereby potentially enabling their observed resistance. Such an astrocyte-specific osmoregulation might thus explain the unaltered localization of TNPO and its cargo, whereas it did not prevent alterations in nuclear structure, suggesting that FUS release from nuclear complexes alone cannot explain the disparities (Figure 7).

Intriguingly, this astrocytic resistance is also seen in disease, where pathological inclusions are found in neurons and other glial cells, but not astrocytes, both in ALS-FUS (Mackenzie et al., 2011) and in FTLD-FUS (Figure 7). Many studies have shown that astrocytes are affected in several neurodegenerative diseases and contain insoluble protein inclusions such as tau deposits in FTD (Komori, 1999) or phosphorylated TDP-43 aggregates, specifically in astrocytes in Alexander disease (Walker et al., 2014). Thus, the coinciding fact that astrocytes are spared from FUS/TNPO pathology and from hyperosmolarity-induced mislocalization leads to the attractive hypothesis that osmotic imbalances could play a critical role in disease initiation.

Cytoplasmic Redistribution of FUS as an Initial Step in the Development of FUS Pathology

A "multiple-hit model" has been proposed for the initiation of FUS pathology, postulating that any event resulting in abnormal cytosolic FUS localization, combined with cellular stress or genetic risk factors favoring aggregation, may trigger formation of insoluble FUS inclusions (Dormann et al., 2010). In this context, recruitment of cytosolic FUS to SGs has been widely hypothesized to act as a "second hit," implying that any insult triggering SG formation in the CNS might initiate inclusion formation (Dormann and Haass, 2011). ALS-causing mutations that disrupt the NLS are likely the "first hit," resulting in diffuse cytoplasmic FUS (Scekic-Zahirovic et al., 2016; Vance et al., 2013).

In sporadic FTD-FUS cases, however, the signal that initially renders FUS cytosolic is unclear. Our findings suggest that hyperosmolar pressure might present a specific insult leading to cytoplasmic mislocalization of FUS, a notion strongly supported by the coaggregation of TNPO and FET proteins in FTD-FUS, but not ALS-FUS. Intriguingly, mislocalization of FET proteins upon hypertonic stress mimics the pattern of pathology seen in FTD patients. TAF15 co-localized completely with FUS in our stress regimen, as well as in patient inclusions, whereas smaller amounts of EWS were detected in the cytoplasm upon stress, consistent with the observation that only a portion of FUS inclusions are EWS-positive (Mackenzie and Neumann, 2012). The fact that other TNPO cargo proteins have not been found in pathological inclusions (Neumann et al., 2011), while these also mislocalize upon sorbitol stress, indicates that additional factors may determine final aggregate formation and specificity. One such factor may be their differential response to the "second hit," i.e., incorporation into SGs, despite their cytoplasmic localization. In line with this, two recent studies showed the critical role of RNA-binding specificities in the incorporation of RBPs within phase-separated granules (Langdon et al., 2018; Maharana et al., 2018). Therefore, it is plausible that the distinct RNA-binding specificities of these proteins may lead to their differential incorporation into SGs and eventually into pathological inclusions. Moreover, the strong aggregation propensity (Sun et al., 2011), as well as the potential prion-like properties (Hock and Polymenidou, 2016) of the highly homologous FET proteins, may render them particularly vulnerable to such a "second hit."

What are the conditions that may lead to osmotic imbalance in the human brain? Multiple studies report an increased risk of developing FTD after severe head trauma (Kalkonde et al., 2012; Rosso et al., 2003; Wang et al., 2015). A serious and common complication of traumatic brain injury (TBI) is cerebral edema, defined as increase in brain water content. The treatment of choice for releasing intracranial pressure is hyperosmolar therapy (Ropper, 2012). Infusion of either mannitol or hypertonic saline solutions rapidly raises plasma osmolarity, thereby reducing brain volume. Because both hypertonic saline and mannitol trigger macromolecular crowding and elicit FUS mislocalization, it is tempting to speculate that the reported association of FTD to TBI might be due to the effect of hyperosmolar therapy rather than the head impact itself. This idea is underscored by the fact that FTD-FUS is a sporadic, early-onset

disease (Lee et al., 2013) characterized by cytoplasmic aggregates containing all FET proteins and TNPO (Neumann et al., 2011). Because the implications for public health are significant, further investigation is urgently needed to clarify the consequences of hyperosmolar therapy in the brain.

STAR★METHODS

Detailed methods are provided in the online version of this paper and include the following:

- KEY RESOURCES TABLE
- CONTACT FOR REAGENT AND RESOURCE SHARING
- EXPERIMENTAL MODEL AND SUBJECT DETAILS
  - Cortico-hippocampal brain slice culture
  - NSC derivation and neural differentiation
  - Cell Lines
- METHOD DETAILS
  - Stress and inhibitor experiments
  - Transient transfection and siRNA-mediated knock down
  - Immunofluorescence staining
  - PolyA RNA *in situ* hybridization
  - SDS-PAGE and Immunoblotting
  - Sequential Insolubility Assay
  - Splicing reporter assay
  - Labeling of newly synthesized proteins
  - Image acquisition
  - Patient tissue sections and analysis
- QUANTIFICATION AND STATISTICAL ANALYSIS
  - Image analysis
  - Statistics

SUPPLEMENTAL INFORMATION

Supplemental Information includes seven figures and one table and can be found with this article online at https://doi.org/10.1016/j.celrep.2018.06.094.

ACKNOWLEDGMENTS

We thank Dr. Shuo-Chien Ling (NUS) for providing the GFP-tagged FUS plasmid, Sarah Erni and Julien Weber for technical help with cell culture, and Claudia Scheckel, Asvin Lakkaraju, Manuela Perez Berlanga, and Julia Lüdke for helpful technical advice, discussions, and critical reading of the manuscript. This work was supported by grants awarded to M.P. from the Swiss National Science Foundation (PP00P3_144862), the Human Frontier Science Program (CDA-00058/2012), and the Neuroscience Center Zürich (ZNZ PhD grant). M.P. and M.-D.R. gratefully acknowledge the support of the NCCR RNA & Disease funded by the Swiss National Science Foundation. The research and related results of M.-D.R. were made possible by the support of the NOMIS Foundation.

AUTHOR CONTRIBUTIONS

E.-M.H. and M.P. conceived the study and wrote the manuscript. E.-M.H. performed and analyzed experiments with help from Z.M. and M.-H.P. (organotypic slice cultures and NSC-based neural model) and F.L. and S.S. (biochemistry experiments). S.R. and M.-D.R. performed NSC-34 splicing assay. L.G. and T.L. performed FTLD patient tissue analysis. H.E., D.D., L.D., and L.P. provided important reagents, mice, and critical input on the study. M.P. supervised the entire study. All authors read, edited, and approved the final manuscript.

DECLARATION OF INTERESTS

The authors declare no competing interests.

Received: December 6, 2017
Revised: May 14, 2018
Accepted: June 22, 2018
Published: July 24, 2018

REFERENCES

Anderson, P., and Kedersha, N. (2009). RNA granules: post-transcriptional and epigenetic modulators of gene expression. Nat. Rev. Mol. Cell Biol. *10*, 430–436.

Andersson, M.K., Ståhlberg, A., Arvidsson, Y., Olofsson, A., Semb, H., Stenman, G., Nilsson, O., and Aman, P. (2008). The multifunctional FUS, EWS and TAF15 proto-oncoproteins show cell type-specific expression patterns and involvement in cell spreading and stress response. BMC Cell Biol. *9*, 37.

Arima, H., Yamamoto, N., Sobue, K., Umenishi, F., Tada, T., Katsuya, H., and Asai, K. (2003). Hyperosmolar mannitol simulates expression of aquaporins 4 and 9 through a p38 mitogen-activated protein kinase-dependent pathway in rat astrocytes. J. Biol. Chem. *278*, 44525–44534.

Bentmann, E., Neumann, M., Tahirovic, S., Rodde, R., Dormann, D., and Haass, C. (2012). Requirements for stress granule recruitment of fused in Sarcoma (FUS) and TAR DNA-binding protein of 43 kDa (TDP-43). J. Biol. Chem. *287*, 23079–23094.

Bertolotti, A., Lutz, Y., Heard, D.J., Chambon, P., and Tora, L. (1996). hTAF(II)68, a novel RNA/ssDNA-binding protein with homology to the pro-oncoproteins TLS/FUS and EWS is associated with both TFIID and RNA polymerase II. EMBO J. *15*, 5022–5031.

Bertolotti, A., Melot, T., Acker, J., Vigneron, M., Delattre, O., and Tora, L. (1998). EWS, but not EWS-FLI-1, is associated with both TFIID and RNA polymerase II: interactions between two members of the TET family, EWS and hTAFII68, and subunits of TFIID and RNA polymerase II complexes. Mol. Cell. Biol. *18*, 1489–1497.

Bosco, D.A., Lemay, N., Ko, H.K., Zhou, H., Burke, C., Kwiatkowski, T.J., Jr., Sapp, P., McKenna-Yasek, D., Brown, R.H., Jr., and Hayward, L.J. (2010). Mutant FUS proteins that cause amyotrophic lateral sclerosis incorporate into stress granules. Hum. Mol. Genet. *19*, 4160–4175.

Bounedjah, O., Hamon, L., Savarin, P., Desforges, B., Curmi, P.A., and Pastré, D. (2012). Macromolecular crowding regulates assembly of mRNA stress granules after osmotic stress: new role for compatible osmolytes. J. Biol. Chem. *287*, 2446–2458.

Bowden, H.A., and Dormann, D. (2016). Altered mRNP granule dynamics in FTLD pathogenesis. J. Neurochem. *138* (*Suppl 1*), 112–133.

Brelstaff, J., Lashley, T., Holton, J.L., Lees, A.J., Rossor, M.N., Bandopadhyay, R., and Revesz, T. (2011). Transportin1: a marker of FTLD-FUS. Acta Neuropathol. *122*, 591–600.

Burg, M.B., Ferraris, J.D., and Dmitrieva, N.I. (2007). Cellular response to hyperosmotic stresses. Physiol. Rev. *87*, 1441–1474.

Burke, K.A., Janke, A.M., Rhine, C.L., and Fawzi, N.L. (2015). Residue-by-Residue View of In Vitro FUS Granules that Bind the C-Terminal Domain of RNA Polymerase II. Mol. Cell *60*, 231–241.

Cushman, M., Johnson, B.S., King, O.D., Gitler, A.D., and Shorter, J. (2010). Prion-like disorders: blurring the divide between transmissibility and infectivity. J. Cell Sci. *123*, 1191–1201.

Deng, Q., Holler, C.J., Taylor, G., Hudson, K.F., Watkins, W., Gearing, M., Ito, D., Murray, M.E., Dickson, D.W., Seyfried, N.T., and Kukar, T. (2014). FUS is phosphorylated by DNA-PK and accumulates in the cytoplasm after DNA damage. J. Neurosci. *34*, 7802–7813.

Dmitrieva, N.I., Cai, Q., and Burg, M.B. (2004). Cells adapted to high NaCl have many DNA breaks and impaired DNA repair both in cell culture and in vivo. Proc. Natl. Acad. Sci. USA *101*, 2317–2322.

Dormann, D., and Haass, C. (2011). TDP-43 and FUS: a nuclear affair. Trends Neurosci. *34*, 339–348.

Dormann, D., Rodde, R., Edbauer, D., Bentmann, E., Fischer, I., Hruscha, A., Than, M.E., Mackenzie, I.R.A., Capell, A., Schmid, B., et al. (2010). ALS-associated fused in sarcoma (FUS) mutations disrupt Transportin-mediated nuclear import. EMBO J. *29*, 2841–2857.

Dredge, B.K., and Jensen, K.B. (2011). NeuN/Rbfox3 nuclear and cytoplasmic isoforms differentially regulate alternative splicing and nonsense-mediated decay of Rbfox2. PLoS ONE *6*, e21585.

Ederle, H., and Dormann, D. (2017). TDP-43 and FUS en route from the nucleus to the cytoplasm. FEBS Lett. *591*, 1489–1507.

Ederle, H., Funk, C., Abou-Ajram, C., Hutten, S., Funk, E.B.E., Kehlenbach, R.H., Bailer, S.M., and Dormann, D. (2018). Nuclear egress of TDP-43 and FUS occurs independently of Exportin-1/CRM1. Sci. Rep. *8*, 7084.

Falsig, J., and Aguzzi, A. (2008). The prion organotypic slice culture assay—POSCA. Nat. Protoc. *3*, 555–562.

Falsig, J., Julius, C., Margalith, I., Schwarz, P., Heppner, F.L., and Aguzzi, A. (2008). A versatile prion replication assay in organotypic brain slices. Nature Neuroscience *11*, 109–117.

Finan, J.D., and Guilak, F. (2010). The effects of osmotic stress on the structure and function of the cell nucleus. J. Cell. Biochem. *109*, 460–467.

Guo, L., Kim, H.J., Wang, H., Monaghan, J., Freyermuth, F., Sung, J.C., O'Donovan, K., Fare, C.M., Diaz, Z., Singh, N., et al. (2018). Nuclear-Import Receptors Reverse Aberrant Phase Transitions of RNA-Binding Proteins with Prion-like Domains. Cell *173*, 677–692.e20.

Hock, E.M., and Polymenidou, M. (2016). Prion-like propagation as a pathogenic principle in frontotemporal dementia. J. Neurochem. *138* (*Suppl 1*), 163–183.

Hofweber, M., Hutten, S., Bourgeois, B., Spreitzer, E., Niedner-Boblenz, A., Schifferer, M., Ruepp, M.D., Simons, M., Niessing, D., Madl, T., et al. (2018). Phase Separation of FUS Is Suppressed by Its Nuclear Import Receptor and Arginine Methylation. Cell *173*, 706–719.e13.

Kalkonde, Y.V., Jawaid, A., Qureshi, S.U., Shirani, P., Wheaton, M., Pinto-Patarroyo, G.P., and Schulz, P.E. (2012). Medical and environmental risk factors associated with frontotemporal dementia: a case-control study in a veteran population. Alzheimers Dement. *8*, 204–210.

Katahira, J. (2012). mRNA export and the TREX complex. Biochim. Biophys. Acta *1819*, 507–513.

Kedersha, N., Cho, M.R., Li, W., Yacono, P.W., Chen, S., Gilks, N., Golan, D.E., and Anderson, P. (2000). Dynamic shuttling of TIA-1 accompanies the recruitment of mRNA to mammalian stress granules. J. Cell Biol. *151*, 1257–1268.

Kim, K.K., Adelstein, R.S., and Kawamoto, S. (2009). Identification of neuronal nuclei (NeuN) as Fox-3, a new member of the Fox-1 gene family of splicing factors. J. Biol. Chem. *284*, 31052–31061.

Kino, Y., Washizu, C., Aquilanti, E., Okuno, M., Kurosawa, M., Yamada, M., Doi, H., and Nukina, N. (2011). Intracellular localization and splicing regulation of FUS/TLS are variably affected by amyotrophic lateral sclerosis-linked mutations. Nucleic Acids Res. *39*, 2781–2798.

Komori, T. (1999). Tau-positive glial inclusions in progressive supranuclear palsy, corticobasal degeneration and Pick's disease. Brain Pathol. *9*, 663–679.

Kudo, N., Matsumori, N., Taoka, H., Fujiwara, D., Schreiner, E.P., Wolff, B., Yoshida, M., and Horinouchi, S. (1999). Leptomycin B inactivates CRM1/exportin 1 by covalent modification at a cysteine residue in the central conserved region. Proc. Natl. Acad. Sci. USA *96*, 9112–9117.

Kültz, D., and Chakravarty, D. (2001). Hyperosmolality in the form of elevated NaCl but not urea causes DNA damage in murine kidney cells. Proc. Natl. Acad. Sci. USA *98*, 1999–2004.

Kwiatkowski, T.J., Jr., Bosco, D.A., Leclerc, A.L., Tamrazian, E., Vanderburg, C.R., Russ, C., Davis, A., Gilchrist, J., Kasarskis, E.J., Munsat, T., et al. (2009). Mutations in the FUS/TLS gene on chromosome 16 cause familial amyotrophic lateral sclerosis. Science *323*, 1205–1208.

Lagier-Tourenne, C., Polymenidou, M., and Cleveland, D.W. (2010). TDP-43 and FUS/TLS: emerging roles in RNA processing and neurodegeneration. Hum. Mol. Genet. *19* (*R1*), R46–R64.

Lagier-Tourenne, C., Polymenidou, M., Hutt, K.R., Vu, A.Q., Baughn, M., Huelga, S.C., Clutario, K.M., Ling, S.-C., Liang, T.Y., Mazur, C., et al. (2012). Divergent Roles of ALS-Linked Proteins FUS/TLS and TDP-43 Intersect in Processing Long Pre-mRNAs (Nature Publishing Group).

Langdon, E.M., Qiu, Y., Ghanbari Niaki, A., McLaughlin, G.A., Weidmann, C.A., Gerbich, T.M., Smith, J.A., Crutchley, J.M., Termini, C.M., Weeks, K.M., et al. (2018). mRNA structure determines specificity of a polyQ-driven phase separation. Science *360*, 922–927.

Lee, B.J., Cansizoglu, A.E., Süel, K.E., Louis, T.H., Zhang, Z., and Chook, Y.M. (2006). Rules for nuclear localization sequence recognition by karyopherin beta 2. Cell *126*, 543–558.

Lee, E.B., Russ, J., Jung, H., Elman, L.B., Chahine, L.M., Kremens, D., Miller, B.L., Branch Coslett, H., Trojanowski, J.Q., Van Deerlin, V.M., and McCluskey, L.F. (2013). Topography of FUS pathology distinguishes late-onset BIBD from aFTLD-U. Acta Neuropathol. Commun. *1*, 1–11.

Liang, S.H., and Clarke, M.F. (1999). A bipartite nuclear localization signal is required for p53 nuclear import regulated by a carboxyl-terminal domain. J. Biol. Chem. *274*, 32699–32703.

Ling, S.C., Polymenidou, M., and Cleveland, D.W. (2013). Converging mechanisms in ALS and FTD: disrupted RNA and protein homeostasis. Neuron *79*, 416–438.

Mackenzie, I.R., and Neumann, M. (2012). FET proteins in frontotemporal dementia and amyotrophic lateral sclerosis. Brain Res. *1462*, 40–43.

Mackenzie, I.R.A., Ansorge, O., Strong, M., Bilbao, J., Zinman, L., Ang, L.-C., Baker, M., Stewart, H., Eisen, A., Rademakers, R., and Neumann, M. (2011). Pathological heterogeneity in amyotrophic lateral sclerosis with FUS mutations: two distinct patterns correlating with disease severity and mutation. Acta Neuropathol. *122*, 87–98.

Maharana, S., Wang, J., Papadopoulos, D.K., Richter, D., Pozniakovsky, A., Poser, I., Bickle, M., Rizk, S., Guillén-Boixet, J., Franzmann, T.M., et al. (2018). RNA buffers the phase separation behavior of prion-like RNA binding proteins. Science *360*, 918–921.

Meissner, M., Lopato, S., Gotzmann, J., Sauermann, G., and Barta, A. (2003). Proto-oncoprotein TLS/FUS is associated to the nuclear matrix and complexed with splicing factors PTB, SRm160, and SR proteins. Exp. Cell Res. *283*, 184–195.

Murakami, T., Qamar, S., Lin, J.Q., Schierle, G.S., Rees, E., Miyashita, A., Costa, A.R., Dodd, R.B., Chan, F.T., Michel, C.H., et al. (2015). ALS/FTD Mutation-Induced Phase Transition of FUS Liquid Droplets and Reversible Hydrogels into Irreversible Hydrogels Impairs RNP Granule Function. Neuron *88*, 678–690.

Nakaya, T., Kawai, T., and Suzuki, T. (2009). Metabolic stabilization of p53 by FE65 in the nuclear matrix of osmotically stressed cells. FEBS J. *276*, 6364–6374.

Neumann, M., Rademakers, R., Roeber, S., Baker, M., Kretzschmar, H.A., and Mackenzie, I.R. (2009). A new subtype of frontotemporal lobar degeneration with FUS pathology. Brain *132*, 2922–2931.

Neumann, M., Bentmann, E., Dormann, D., Jawaid, A., DeJesus-Hernandez, M., Ansorge, O., Roeber, S., Kretzschmar, H.A., Munoz, D.G., Kusaka, H., et al. (2011). FET proteins TAF15 and EWS are selective markers that distinguish FTLD with FUS pathology from amyotrophic lateral sclerosis with FUS mutations. Brain *134*, 2595–2609.

Pankiv, S., Lamark, T., Bruun, J.A., Øvervatn, A., Bjørkøy, G., and Johansen, T. (2010). Nucleocytoplasmic shuttling of p62/SQSTM1 and its role in recruitment of nuclear polyubiquitinated proteins to promyelocytic leukemia bodies. J. Biol. Chem. *285*, 5941–5953.

Patel, A., Lee, H.O., Jawerth, L., Maharana, S., Jahnel, M., Hein, M.Y., Stoynov, S., Mahamid, J., Saha, S., Franzmann, T.M., et al. (2015). A Liquid-to-Solid Phase Transition of the ALS Protein FUS Accelerated by Disease Mutation. Cell *162*, 1066–1077.

Qamar, S., Wang, G., Randle, S.J., Ruggeri, F.S., Varela, J.A., Lin, J.Q., Phillips, E.C., Miyashita, A., Williams, D., Strohl, F., et al. (2018). FUS Phase Separation Is Modulated by a Molecular Chaperone and Methylation of Arginine Cation-pi Interactions. Cell *173*, 720–734.e15.

Raczynska, K.D., Ruepp, M.D., Brzek, A., Reber, S., Romeo, V., Rindlisbacher, B., Heller, M., Szweykowska-Kulinska, Z., Jarmolowski, A., and Schumperli, D. (2015). FUS/TLS contributes to replication-dependent histone gene expression by interaction with U7 snRNPs and histone-specific transcription factors. Nucleic Acids Research *43*, 9711–9728.

Rappsilber, J., Ryder, U., Lamond, A.I., and Mann, M. (2002). Large-scale proteomic analysis of the human spliceosome. Genome Res. *12*, 1231–1245.

Reber, S., Stettler, J., Filosa, G., Colombo, M., Jutzi, D., Lenzken, S.C., Schweingruber, C., Bruggmann, R., Bachi, A., Barabino, S.M., et al. (2016). Minor intron splicing is regulated by FUS and affected by ALS-associated FUS mutants. EMBO J. *35*, 1504–1521.

Risher, W.C., Andrew, R.D., and Kirov, S.A. (2009). Real-time passive volume responses of astrocytes to acute osmotic and ischemic stress in cortical slices and in vivo revealed by two-photon microscopy. Glia *57*, 207–221.

Ropper, A.H. (2012). Hyperosmolar therapy for raised intracranial pressure. N. Engl. J. Med. *367*, 746–752.

Rosso, S.M., Landweer, E.J., Houterman, M., Donker Kaat, L., van Duijn, C.M., and van Swieten, J.C. (2003). Medical and environmental risk factors for sporadic frontotemporal dementia: a retrospective case-control study. J. Neurol. Neurosurg. Psychiatry *74*, 1574–1576.

Sama, R.R., Ward, C.L., Kaushansky, L.J., Lemay, N., Ishigaki, S., Urano, F., and Bosco, D.A. (2013). FUS/TLS assembles into stress granules and is a prosurvival factor during hyperosmolar stress. J. Cell. Physiol. *228*, 2222–2231.

Scekic-Zahirovic, J., Sendscheid, O., El Oussini, H., Jambeau, M., Sun, Y., Mersmann, S., Wagner, M., Dieterlé, S., Sinniger, J., Dirrig-Grosch, S., et al. (2016). Toxic gain of function from mutant FUS protein is crucial to trigger cell autonomous motor neuron loss. EMBO J. *35*, 1077–1097.

Schwartz, J.C., Ebmeier, C.C., Podell, E.R., Heimiller, J., Taatjes, D.J., and Cech, T.R. (2012). FUS binds the CTD of RNA polymerase II and regulates its phosphorylation at Ser2. Genes Dev. *26*, 2690–2695.

Sheikh-Hamad, D., and Gustin, M.C. (2004). MAP kinases and the adaptive response to hypertonicity: functional preservation from yeast to mammals. Am. J. Physiol. Renal Physiol. *287*, F1102–F1110.

Shin, H.J., Kim, H., Heo, R.W., Kim, H.J., Choi, W.S., Kwon, H.M., and Roh, G.S. (2014). Tonicity-responsive enhancer binding protein haplodeficiency attenuates seizure severity and NF-kappaB-mediated neuroinflammation in kainic acid-induced seizures. Cell Death Differ. *21*, 1095–1106.

Sloan, K.E., Gleizes, P.E., and Bohnsack, M.T. (2016). Nucleocytoplasmic Transport of RNAs and RNA-Protein Complexes. J. Mol. Biol. *428* (*10 Pt A*), 2040–2059.

Sun, Z., Diaz, Z., Fang, X., Hart, M.P., Chesi, A., Shorter, J., and Gitler, A.D. (2011). Molecular determinants and genetic modifiers of aggregation and toxicity for the ALS disease protein FUS/TLS. PLoS Biol. *9*, e1000614.

Sun, S., Ling, S.C., Qiu, J., Albuquerque, C.P., Zhou, Y., Tokunaga, S., Li, H., Qiu, H., Bui, A., Yeo, G.W., et al. (2015). ALS-causative mutations in FUS/TLS confer gain and loss of function by altered association with SMN and U1-snRNP. Nat. Commun. *6*, 6171.

Timney, B.L., Raveh, B., Mironska, R., Trivedi, J.M., Kim, S.J., Russel, D., Wente, S.R., Sali, A., and Rout, M.P. (2016). Simple rules for passive diffusion through the nuclear pore complex. J. Cell Biol. *215*, 57–76.

Trask, D.K., and Muller, M.T. (1988). Stabilization of type I topoisomerase-DNA covalent complexes by actinomycin D. Proc. Natl. Acad. Sci. USA *85*, 1417–1421.

Vance, C., Rogelj, B., Hortobágyi, T., De Vos, K.J., Nishimura, A.L., Sreedharan, J., Hu, X., Smith, B., Ruddy, D., Wright, P., et al. (2009). Mutations in FUS, an RNA processing protein, cause familial amyotrophic lateral sclerosis type 6. Science *323*, 1208–1211.

Vance, C., Scotter, E.L., Nishimura, A.L., Troakes, C., Mitchell, J.C., Kathe, C., Urwin, H., Manser, C., Miller, C.C., Hortobágyi, T., et al. (2013). ALS mutant FUS disrupts nuclear localization and sequesters wild-type FUS within cytoplasmic stress granules. Hum. Mol. Genet. *22*, 2676–2688.

Walker, A.K., Daniels, C.M., Goldman, J.E., Trojanowski, J.Q., Lee, V.M., and Messing, A. (2014). Astrocytic TDP-43 pathology in Alexander disease. J. Neurosci. *34*, 6448–6458.

Wang, H.K., Lee, Y.C., Huang, C.Y., Liliang, P.C., Lu, K., Chen, H.J., Li, Y.C., and Tsai, K.J. (2015). Traumatic brain injury causes frontotemporal dementia and TDP-43 proteolysis. Neuroscience *300*, 94–103.

Wippich, F., Bodenmiller, B., Trajkovska, M.G., Wanka, S., Aebersold, R., and Pelkmans, L. (2013). Dual specificity kinase DYRK3 couples stress granule condensation/dissolution to mTORC1 signaling. Cell *152*, 791–805.

Wühr, M., Güttler, T., Peshkin, L., McAlister, G.C., Sonnett, M., Ishihara, K., Groen, A.C., Presler, M., Erickson, B.K., Mitchison, T.J., et al. (2015). The nuclear proteome of a vertebrate. Curr. Biol. *25*, 2663–2671.

Yi, M.H., Lee, Y.S., Kang, J.W., Kim, S.J., Oh, S.H., Kim, Y.M., Lee, Y.H., Lee, S.D., and Kim, D.W. (2013). NFAT5-dependent expression of AQP4 in astrocytes. Cell. Mol. Neurobiol. *33*, 223–232.

Yoshizawa, T., Ali, R., Jiou, J., Fung, H.Y.J., Burke, K.A., Kim, S.J., Lin, Y., Peeples, W.B., Saltzberg, D., Soniat, M., et al. (2018). Nuclear Import Receptor Inhibits Phase Separation of FUS through Binding to Multiple Sites. Cell *173*, 693–705.e22.

Zhang, Z.C., and Chook, Y.M. (2012). Structural and energetic basis of ALS-causing mutations in the atypical proline-tyrosine nuclear localization signal of the Fused in Sarcoma protein (FUS). Proc. Natl. Acad. Sci. USA *109*, 12017–12021.

Zhou, Z., Licklider, L.J., Gygi, S.P., and Reed, R. (2002). Comprehensive proteomic analysis of the human spliceosome. Nature *419*, 182–185.

Zinszner, H., Albalat, R., and Ron, D. (1994). A novel effector domain from the RNA-binding protein TLS or EWS is required for oncogenic transformation by CHOP. Genes Dev. *8*, 2513–2526.

STAR★METHODS

KEY RESOURCES TABLE

REAGENT or RESOURCE	SOURCE	IDENTIFIER
Antibodies		
Alexa 488 donkey anti-chicken	Jackson Laboratories	Cat# 703-546-155, RRID:AB_2340376
Alexa 488 donkey anti-goat	Life Technologies	Cat# A-11055, RRID:AB_2534102
Alexa 488 donkey anti-mouse	Life Technologies	Cat# A-21202, RRID:AB_141607
Alexa 488 donkey anti-rabbit	Life Technologies	Cat# A-21206, RRID:AB_2535792
Alexa 568 goat anti-rabbit	Invitrogen	Cat# A-11011, RRID:AB_143157
Alexa 594 donkey anti-mouse	Life Technologies	Cat# A-21203, RRID:AB_2535789
Alexa 594 donkey anti-rabbit	Life Technologies	Cat# A-21207, RRID:AB_141637
Alexa 647 donkey anti-chicken	Jackson Laboratories	Cat# 703-606-155, RRID:AB_2340380
Alexa 647 donkey anti-goat	Life Technologies	Cat# A-21447, RRID:AB_2535864
Alexa 647 donkey anti-mouse	Life Technologies	Cat# A-31571, RRID:AB_162542
Alexa 647 donkey anti-rabbit	Life Technologies	Cat# A-31573, RRID:AB_2536183
Anti-actin	Sigma Aldrich	Cat# A5060, RRID:AB_476738
Anti-CD68	AbD Serotec	Cat#MCA1957
Anti-eIF3η	Santa Cruz	Cat# sc-16377, RRID:AB_671941
Anti-ERK	CST	Cat# 9102, RRID:AB_330744
Anti-EWS	Santa Cruz	Cat# sc-28327, RRID:AB_675526
Anti-FLAG	Thermofisher	Cat# MA1-91878, RRID:AB_1957945
Anti-FLAG	Sigma-Aldrich	Cat# F1804, RRID:AB_262044
Anti-FUS	Bethyl	Cat# A300-293A, RRID:AB_263409
Anti-FUS	Bethyl	Cat# A300-294A, RRID:AB_263410
Anti-FUS	Santa Cruz	Cat# sc-47711, RRID:AB_2105208
Anti-FUS	homemade (Raczynska et al., 2015)	N/A
Anti-G3BP	Abcam	Cat# ab56574, RRID:AB_941699
Anti-GAPDH	Abcam	Cat# ab8245, RRID:AB_2107448
Anti-GFAP	Dako	Cat# Z0334, RRID:AB_10013382
Anti-GFAP (only for IHC)	Abcam	Cat# ab53554, RRID:AB_880202
Anti-GFP-FITC	Rockland antibodies	Cat# 600-102-215, RRID:AB_218187
Anti-HA	Proteintech	Cat#66006-1-Ig
Anti-hnRNPA1	Abcam	Cat# ab5832, RRID:AB_305145
Anti-hnRNPA2B1	Abcam	Cat# ab6102, RRID:AB_305293
Anti-hnRNPU	Novus biologicals	Cat#NBP2-49290
Anti-Imp7	Bethyl	Cat# A302-727A, RRID:AB_10627807
Anti-MAP2	Sigma	Cat# M1406, RRID:AB_477171
Anti-MOG	Abcam	Cat# ab32760, RRID:AB_2145529
Anti-NEFM	Thermofisher	Cat# 13-0700, RRID:AB_2532998
Anti-NEUN	Millipore	Cat# ABN91, RRID:AB_11205760
Anti-p38	CST	Cat# 9212, RRID:AB_330713
Anti-p53	CST	Cat# 2527S, RRID:AB_10695803
Anti-phATF2	CST	Cat# 9221, RRID:AB_2561045
Anti-phERK	CST	Cat# 9102, RRID:AB_330744
Anti-phJNK	CST	Cat# 9251, RRID:AB_331659
Anti-SOD1	Enzo Life Sciences	Cat# ADI-SOD-100, RRID:AB_10616253
Anti-TAF15	Abcam	Cat# ab134916, RRID:AB_2614922

(*Continued on next page*)

Continued

REAGENT or RESOURCE	SOURCE	IDENTIFIER
Anti-TDP-43	Antibodies online	Cat#ABIN487384
Anti-TIA-1	Santa Cruz	Cat# sc-1751, RRID:AB_2201433
Anti-TIAR	BD Bioscience	Cat# 610352, RRID:AB_397742
Anti-TNPO1	Sigma	Cat# T0825, RRID:AB_262123
Anti-TNPO1 (only for IHC)	Abcam	Cat# ab10303, RRID:AB_2206878
Anti-TNPO2	Proteintech	Cat# 17831-1-AP, RRID:AB_10598481
Anti-TonEBP/NFAT5	Santa Cruz	Cat# sc-398171
Anti-VIM	Millipore	Cat# AB5733, RRID:AB_11212377
Anti-β-ACTIN	Sigma	Cat# A5441, RRID:AB_476744
Anti-β-TUB	Sigma	Cat# T4026, RRID:AB_477577
HRP-conjugated goat anti-mouse	Jackson Laboratories	Cat# 115-035-146, RRID:AB_2307392
HRP-conjugated goat anti-rabbit	Jackson Laboratories	Cat# 111-035-144, RRID:AB_2307391
IRDye® 800CW Goat anti-rabbit	LI-COR	P/N 925-32211
Biological Samples		
aFTLD-FUS patient material	Queen Square Brain Bank for Neurological diseases	N/A
NIFID FUS patient material	Queen Square Brain Bank for Neurological diseases	N/A
Chemicals, Peptides, and Recombinant Proteins		
5,6-Dichlorobenzimidazole 1-β-D-ribofuranoside	Sigma	Cat# D1916
Actinomycin	Sigma	Cat# A1410
Adox	Sigma	Cat# A7154
AffinityScript Multiple Temperature	Agilent Technologies	Cat #200436
BDNF	PeproTech	Cat#450-02
Benzonase	Millipore	Cat# 71205-3
BME with Earles salt sol., w/o L-Glutamine	Life Technologies	Cat# 41010-109
CNTF	Alomone lab	Cat# C-240
Complete protease inhibitor cocktail	Roche	Cat# 11873580001
Cycloheximide	Sigma	Cat# C4859
DAPI	Sigma	Cat# D9542
Dexamethasone	Sigma	Cat# D4902
DMEM-F12	Life Technologies	Cat# 31330095
Donkey serum	Millipore	Cat# S30
Earle's salt solution	Life Technologies	Cat# 14155-048
Ec23	Amsbio	Cat# AMS.SRP002-2
Emetine	Sigma	Cat# E2375
Forskolin	Cayman	Cat# AG-CN2-0089-M050
GDNF	PeproTech	Cat#450-10
GlutaMAX	Life Technologies	Cat# 35050038
Gö 6983	Sigma	Cat# G1918
GSK-626616	L. Pelkmans	N/A
Heat inactivated horse serum	GIBCO	Cat# 26050-088
Kynurenic acid	Sigma	Cat# K3375
Leptomycin B	Sigma	Cat# L2913
Matrigel	Corning	Cat #354234
MESA GREEN qPCR Mastermix	Eurogentec	05-SY2X-03+NRWOU
Methionine-free DMEM medium	Life Technologies	Cat# 21013-024

(*Continued on next page*)

Continued

REAGENT or RESOURCE	SOURCE	IDENTIFIER
N2	Life Technologies	Cat# 17502001
Nu 7441	Selleckchem	Cat# S2638
NuPAGE LDS Sample Buffer (4X)	ThermoFisher Scientific	NP0007
Penicillin/streptomycin	GIBCO	Cat# 15140122
PhosStop	Roche	Cat# 04906845001
RIPA Lysis and Extraction Buffer	ThermoFisher Scientific	89900
SAG	Millipore	Cat# 566660
Saline sodium citrate	Sigma	Cat# S6639
Sarkosyl	Sigma	Cat# L5125
SB202119	Abcam	ab120638
SB203580	R&D Systems	Cat# 1202
SKI-1	Abcam	ab120839
Sodium arsenite	Sigma	Cat# S7400
Sorbitol	Sigma	Cat# S7547
SP600125	Sigma	Cat# S5567
Staurosporine	Sigma	Cat# S6942
Sucrose	Sigma	Cat# 84100
Urea	Sigma	Cat# 51456
Wortmannin	Sigma	Cat# W1628
Critical Commercial Assays		
Lipofectamine®2000 Transfection Reagent	Life Technologies	Cat# 11668019
Click-IT AHA	ThermoFisher Scientific	Cat# C10102
Click-IT TAMRA Protein Analysis Detection Kit	ThermoFisher Scientific	Cat# C33370
TURBO DNA-free Kit	ThermoFisher Scientific	AM1907
TSA fluorescein kit	Perkin-Elmer	
Experimental Models: Cell Lines		
NSC-34	Cedarlane	Cat#CLU140, RRID:CVCL_D356
SHSY5Y	M. Ruepp	N/A
HEK293	A. Aguzzi	N/A
Experimental Models: Organisms/Strains		
Mice C57BL/6J	Janvier	Cat#C57BL/6JRj
Oligonucleotides		
Aly/REF	Dharmacon siGENOME SMARTpools	Cat# M-046521-00-0005
TonEBP	Microsynth; Shin et al., 2014	N/A
oligo(dT)30-Cy3 probe	Microsynth	N/A
Primers for qPCR	this paper, Reber et al., 2016	N/A
Recombinant DNA		
pcDNA6-Flag-FUS	M. Ruepp	N/A
GFP-FUS	Sun et al., 2015	N/A
pCMV-SCN4A	Reber et al., 2016	N/A
pcDNA3.1(+)	ThermoFisher Scientific	V79020
Software and Algorithms		
ImageJ	NIH, USA	https://imagej.nih.gov/ij/download.html
GraphPad Prism 7	GraphPad Prism Software, Inc	https://www.graphpad.com/scientific-software/prism/

(*Continued on next page*)

Continued

REAGENT or RESOURCE	SOURCE	IDENTIFIER
Other		
Tissue chopper	McIlwain	Cat# TC752
Minilys device	Bertin	Cat# Equation 06404-200-RD000.0
Bolt 12% Bis-Tris gels	Life Technologies	NW00122BOX
iBlot 2	Life Technologies	IB21001
IBlot2 transfer stacks, NC, regular	Life Technologies	IB23001
Inverted Leica confocal microscope	Leica	SP5 APD
Leica fluorescence microscope	Leica	DM5500B
Millicell-CM inserts	Millipore	PICM03050
Rotorgene6000	Corbett	N/A

CONTACT FOR REAGENT AND RESOURCE SHARING

Further information and requests for resources and reagents should be directed to and will be fulfilled by the Lead Contact, Magdalini Polymenidou (magdalini.polymenidou@imls.uzh.ch).

EXPERIMENTAL MODEL AND SUBJECT DETAILS

Cortico-hippocampal brain slice culture

Cortico-hippocampal brain slice preparation was adapted from previously published protocols (Falsig and Aguzzi, 2008; Falsig et al., 2008). Slices were prepared from 5-8 day old C57BL/6J pups. After decapitation the brain was removed quickly under sterile conditions and placed in a drop of ice cold GBSSK (137 mM NaCl, 5 mM KCl, 0.845 mM Na_2HPO_4, 1.5 mM $CaCl_2$ x $2H_2O$, 0.66 mM KH_2PO_4, 0.28 mM $MgSO_4$ x $7H_2O$, 1 mM $MgCl_2$ x $6H_2O$, 2.7 mM NaHCO3, 33.33 mM Glucose, 1 mM kynurenic acid, pH to 7.2–7.4). The hippocampus plus the surrounding cortical regions were dissected under a binocular and placed on a tissue chopper in an orientation that the hippocampus lies stretched out in a 90 degree angle to the cutting blade with the cortical parts on top. 350 nm slices were cut and separated under the binocular in GBSSK. Two slices each were placed in Millicell-CM inserts in 6 well plates, residual GBSSK was removed, cold forebrain culture medium was added to the bottom of the well and the plate was moved to the incubator. Medium was changed the following day to remove residual buffer. Slice cultures were maintained in forebrain culture medium (50% BME with Earles salt sol., w/o L-Glutamine, 25% Earle's salt solution, 25% heat inactivated horse serum, supplemented with 1% glucose, 1% penicillin/streptomycin and GlutaMAX C in a humidified incubator at 37°C with 5% CO_2 for at least 3 weeks before the start of the experiment to stabilize after preparation.

Mice housing and breeding were in accordance with the Swiss Animal Welfare Law and in compliance with the regulations of the Cantonal Veterinary Office, Zurich.

NSC derivation and neural differentiation

iPSC and NSC derivation and their differentiation into neurons and astrocytes will be described in detail in *Hruska-Plochan et al.* (manuscript under review). Briefly, iPSCs were generated from control human early post natal dermal fibroblasts via episomal reprogramming using plasmids coding for Oct3/4, Sox2, Klf4 and p53-shRNA. Resulting iPSC colonies were manually picked and cultured in non-adhesive conditions to generate embryoid bodies which upon plating onto poly-L-ornithine/laminin coated plastic in NSC medium containing bFGF induced the formation of neuronal rosettes. These were manually dissected and enriched via three consecutive passaging steps. Patches of cells with a distinct morphology migrating out of the neuronal rosettes were then manually picked and considered neuronal stem cell clones, which were expanded for future differentiation. For experiments, NSCs were differentiated into neuronal cultures for 25 days using Forskolin, Ec23 and SAG with the addition of BDNF, GDNF and CNTF from day 11 on. After 25 days cells were subcultured and recovered in D3 medium. At this point the neural culture already contains neurons, astrocytes and oligodendrocytes. To obtain pure astrocytic cultures cells from the differentiated neural cultures were replated in astrocyte medium at day 25 and remaining neurons were killed off via 2-3 passages. For experiments, astrocytes were plated sparsely which promotes their maturation.

Post-differentiation astrocytes and neural cultures were cultured on Matrigel (230μg/ml) in astrocyte medium (DMEM-F12, 1% N2, 0.2% penicillin/streptomycin, 1% GlutaMAX, 20ng/ml CNTF) or 'D3 medium' (DMEM-F12, 1% B27+, 1% GlutaMAX, 20ng/ml BDNF, 20ng/ml GDNF, 20ng/ml CNTF, 1% N2, 1% penicillin/streptomycin) respectively in a humidified incubator at 37°C with 5% CO_2.

Cell Lines

Cells were maintained in a humidified incubator at 37°C with 5% CO_2. HEK293, NSC-34 and SHSY5Y cells were grown in DMEM-F12 with 10% FBS and 1% penicillin/streptomycin. 2-5 days prior to experiments, NSC-34 were switched to differentiation medium (DMEM-F12, 1% B27+, 1% GlutaMAX, 10ng/ml BDNF, 10ng/ml GDNF, 1% N2, 0.2% penicillin/streptomycin) and grown on Matrigel (90μg/ml) coated culture dishes.

METHOD DETAILS

Stress and inhibitor experiments

For stress experiments, sorbitol, urea, and sucrose were directly dissolved in the medium to add an additional osmolarity of 0.4M. To reach hypoosmolar conditions medium without Earls salts was used. To induce oxidative stress, 0.25-0.5mM sodium arsenite was added to the medium. Different compounds were used at indicated concentrations in the culture medium: cycloheximide (100μg/ml), emetine (100μM), GSK-626616 (50μM), actinomycin (5μg/ml), DRB (5,6-Dichlorobenzimidazole 1-β-D-ribofuranoside, 10μM), Adox (20mM), SB202119 (20μM), SB203580 (20μM), SKI (20μM), wortmannin (5μM), SP600125 (20μM), Gö 6983 (5μM), leptomycin B (10n), staurosporine (1μM), Nu 7441 (1μM). In case of inhibitor treatment parallel with stress experiments, all inhibitor compounds were added 15 min prior to the start of the stress insult except otherwise indicated. To induce nuclear import of GR2-GFP2-fusion proteins, cells were incubated for 20 min with dexamethasone (5μM).

Transient transfection and siRNA-mediated knock down

Transient plasmid transfections were achieved using Lipofectamine®2000 Transfection Reagent according to manufacturer's protocol with 1ng/μl DNA. siRNA transfections were performed with Lipofectamine®2000 at a final concentration of 25nM siRNA or 40nM (TonEBP). Culture medium was exchanged 24h after transfection and the knock down was analyzed 48h post-transfection by immunoblotting and immunostaining.

Immunofluorescence staining

For immunostaining cultures were first fixed in 4% Formaldehyde in PBS for 10 min (cells) and overnight (ON) (slices). After washing, permeabilization and blocking buffer (10% donkey serum and 0.3% Triton X-100 in PBS) was added for 1h (cells) or 4h (slices). Primary antibodies were added in blocking buffer and incubated for approximately 2h at room temperature (RT) or ON at 4°C for cells or 2-3 days for slices (see antibody list). Cultures were washed three times in PBS before incubating them with 488-, 594 or 647-Alexa-conjugated secondary antibodies raised in donkey (1:1000) for 1h at RT (cells) or ON at 4°C (slices) and subsequently washed with PBS. For slice cultures, additional DAPI (1μg/ml) was added for 30 min in PBS. After washing, cells and slices were mounted with mounting medium anti-fade with DAPI and left to harden at RT for at least 24h in the dark before imaging.

PolyA RNA *in situ* hybridization

Cells were fixed for 10 min at RT in 4% formaldehyde in PBS, washed in FISH buffer (2X saline sodium citrate (SSC) with 10% Formamide, then permeabilized for 30 min in 0.1% Triton X-100 and 0.1% BSA in FISH buffer. After washing in FISH buffer, hybridization with 0.5μM oligo$(dT)_{30}$-Cy3 probe was carried out for 4 h at 37°C, followed by a washing step at 37°C in FISH buffer. Subsequently, immunostaining with primary antibodies was carried as mentioned above, with PBS exchanged to SSC buffer at all steps.

SDS-PAGE and Immunoblotting

Cells were scraped in ice cold lysis buffer with Benzonase and 2mM $MgCl_2$ and homogenates were cleared 5 min at 17 000 g. To collect slice tissue, several brain slices were scraped into lysis buffer with Benzonase and 2mM $MgCl_2$ and subjected to 2 times 30 s of homogenization at full speed with a Minilys device in tubes containing ceramic beads. Protein concentration was adjusted based on BCA assay and lysates were boiled in loading buffer with reducing agent before loading the samples on Bolt 12% Bis-Tris gels. For immunoblots, gels were transferred onto nitrocellulose membranes using iBlot 2, which were blocked with 5% non-fat skimmed powder milk in PBS-Tween and probed with primary antibodies ON (see list) followed by secondary HRP-conjugated goat anti mouse or rabbit IgG antibodies (1:5000, 1:10000, respectively). Immunoreactivity was visualized by chemiluminescence.

Sequential Insolubility Assay

Slice tissue was subjected to increasing detergent stringency (1. salt buffer, 2. RIPA, 3. 1% Triton-X, 4. 2% Sarkosyl) separating soluble and insoluble material after each step via centrifugation. Initially, slices were scraped in salt buffer (10mM Tris, 250mM NaCl, 1mM EDTA, 1mM DTT, complete protease inhibitor cocktail, PhosStop) containing Benzonase and 2mM $MgCl_2$ and homogenized using Minilys for twice 30 s at full speed followed by a 30 min centrifugation step at 4°C with 17 000 g. The supernatant was collected and the pellet was resuspended in salt buffer containing RIPA detergents with Benzonase and MgCl2. After 30 min

incubation, pellet and supernatant were separated again by centrifugation. This process was repeated until a sarkosyl-insoluble pellet was obtained, which was dissolved in original volume of loading buffer and subjected to immunoblotting with all other samples as described above.

Splicing reporter assay

Cells were co-transfected with 400 ng of the SCN4A reporter plasmid and 600 ng empty filler plasmid (pcDNA3.1(+)) using Lipofectamine 2000 according to the manufacturer's instructions. After 48h cells were stressed for 2h with 0.4M sorbitol. Thereafter, half of the cells were harvested using Trizol for subsequent standard RNA isolation. The purified RNA was DNase treated using the TURBO DNA-free according to the manufacturer's manual. Reverse transcription of total RNA was performed using the AffinityScript Multiple Temperature cDNA Synthesis Kit according to the manufacturer's manual. RT-qPCR was performed using 3 μl cDNA, 1 x MESA GREEN qPCR Mastermix Plus for SYBRR Assay No ROX and each 8 μl forward and reverse primer in a total volume of 15 μl per reaction. qPCR primers for SCN4A were used as published in Reber et al., 2016 and primers for control genes are listed in Table S1 in Supplemental Information. Samples were measured in duplicates in a Rotorgene6000. The following cycling conditions were used: 95°C, 5 min; 95°C, 15 s; 60°C 1 min; 40 cycles. A melting curve was recorded from a temperature gradient from 65°C to 95°C, 5 s/°C. Analysis was performed using the Rotor-Gene 6000 Series Software V1.7. The other half of the cells were lysed using RIPA buffer. The lysate was centrifuged 15 min at 16'000 g at 4°C to remove insoluble components and the supernatant was re-suspended in 4X LDS-loading buffer for subsequent SDS-PAGE western blot analysis with the primary antibodies (rabbit anti-actin (Sigma Aldrich, A 5060) or rabbit anti-FUS (homemade, (Raczynska et al., 2015)), respectively) and with fluorescence-labeled secondary antibody (IRDye® 800CW Goat anti-Rabbit IgG (H + L)). Membranes were analyzed with the Odyssey Infrared Imaging System.

Labeling of newly synthesized proteins

Newly synthesized proteins were labeled using a combination of the Click-IT AHA and the Click-IT TAMRA Protein Analysis Detection Kit according to the manufacturer's protocol. Briefly, cells were washed in PBS and methionine-free DMEM medium was added for 45 min after which translation inhibitors were added to the medium for 15 min prior to addition of AHA (50μM, L-Azidohomoalanine) for 1h. Cells were then fixed for 10 min, washed in PBS and permeabilized in 0.25% Triton-X, 1% BSA in PBS. After washing in 3% BSA in PBS the TAMRA reaction mix was added for 30 min protected from light. Samples were then subjected to additional antibody staining as described.

Image acquisition

All confocal microscopy except for patient tissue section analysis was performed at the ZMB core facility of the University of Zuerich with an inverted Leica SP5 microscope, equipped with lasers for 405, 488, 561 and 633 nm excitation. Images were acquired using 48-fold line averaging with a 40x1.25 or 63x1.4 oil objective at different zooms. Settings were kept identical between groups of samples within an experiment. For quantification neuron and NSC-34 images were taken with 63x1.4 objective at 1.7x zoom, slice images with 63x1.4 objective at 4x zoom and astrocyte images with 40x1.25 objective at 1.7x zoom; exception: For quantification of FUS and polyA mRNA in the Aly/REF knock down experiment single cells with successful KD (nuclear retained mRNA and reduced Aly/REF levels) were imaged with 63x1.4 objective at 8x zoom.

Patient tissue sections and analysis

Patient material has been collected from donors for or from whom a written informed consent for a brain autopsy and the use of the material and clinical information for research purposes has been obtained by the Queen Square Brain Bank for Neurological diseases. In total, hippocampus, frontal and temporal cortices of four FTLD-FUS cases (2 NIFID and 2 aFTLD-FUS) were analyzed. 8 μm thick tissue sections were cut from paraffin embedded tissue. Endogenous peroxidase activity was blocked with 0.3% H_2O_2 in methanol followed by pressure cooker pre-treatment in citrate buffer pH 6.0. Sections were treated with 10% dried milk solution to block non-specific binding. Tissue sections were incubated with the primary anti-TNPO1 (Abcam, 1:200) antibody for 1 hr at room temperature, followed by biotinylated anti-mouse (Dako; 1:200), ABC complex (Dako) and visualized using TSA fluorescein kit. Sections were then incubated with anti-GFAP (Dako, 1:1000) for 1 hr at room temperature followed by the secondary anti-rabbit Alexa Fluor 568 (1:500). Sections were counterstained with 4'-6-diamidino-2-phenylindol (DAPI) and viewed under a Leica DM5500B fluorescence microscope using 3D deconvolution post-processing.

QUANTIFICATION AND STATISTICAL ANALYSIS

Image analysis

To measure FUS (or other proteins/mRNA) amounts outside of the nucleus a threshold was applied to DAPI and FUS frames. The thresholded DAPI mask was subtracted from the FUS image. Positive pixels of the resulting image containing only non-nuclear FUS pixels were measured and given as a percentage of the overall FUS pixels in the original image. For slice image quantification, only pixels overlaying with the neuronal marker NEUN were taken into calculation. For TNPO quantification in neurons this percentage was additionally normalized to TNPO positive area. Images for quantification were thresholded independently for each experiment to achieve similar values for the non-treated control condition. Achieved percentages represent arbitrary values for comparison

and not absolute numbers. Figures are displayed as box and whisker graphs except otherwise indicated together with the number of images (n) in the respective figure legends.

Statistics

The statistical significance of two groups of results was determined by a two-tailed, unpaired t test (except paired t test for densitometrical quantification of immunoblots) using GraphPad Prism 7.